Electrical Engineering
https://doi.org/10.1007/s00202-023-02171-0

ORIGINAL PAPER

Multi-objective combined heat and power with wind–solar–EV of optimal power flow using hybrid evolutionary approach

Chandan Paul[1] · Tushnik Sarkar[1] · Susanta Dutta[1] · Provas Kumar Roy[2]

Received: 25 June 2023 / Accepted: 28 November 2023

Abstract

The proposed effort aims to investigate efficient power generation while minimizing emissions, voltage deviations, and maintaining transmission line voltage stability. The combined heat and power of economic dispatch (CHPED) system is incorporated in the IEEE-57 bus in this presentation to ensure the best possible power flow in the transmission line while meeting the load demand. It is crucial to incorporate renewable energy sources for efficient power generation because fossil fuel sources are evolving daily. The main contribution of the proposed work is firstly, to find optimal solution for optimal power flow (OPF)-based combined heat and power economic dispatch (CHPED) problem with wind, solar and electric vehicles (EVs). The target is to find out maximum utilization of renewable energy sources for economic power generation, less emission and reduced transmission losses with maintaining the permissible voltage deviation at load buses. Thus, a new approach of electric vehicle to grid has been adopted with wind–solar-CHPED-based OPF system for improving grid reliability and resilience. Secondly, there is a requirement to overcome the local optima problems having low convergence speed. This is obtained by employing a relatively new methodology, known as chaotic-opposition-based driving training-based optimization (DTBO) (CODTBO). Due to the presence of wind, solar, EVs uncertainties, valve point effect, and transmission losses, the system grew more complex. For three different test systems for CHPED-based OPF with and without RESs, the proposed CODTBO algorithm has been put to the test. Results from the tested DTBO, ODTBO approach and the proposed CODTBO have been compared. After integrating wind–solar–EVs with CHPED–OPF, the total fuel cost and emission are reduced by 3.48% and 5.1%, respectively, as well as L-index is improved by 21.6%. Hence, it has been proved that proposed CODTBO has the capability to easily cope up with nonlinear functions. After adding chaotic-oppositional-based learning (CO) with DTBO (CODTBO), the fuel cost is further reduced by 1.65% and computational time is improved by 45% as compared to DTBO. Henceforth, CODTBO has the better exploration capability and better searching ability as compared to DTBO. The above numerical analysis demonstrated the superiority of the suggested CODTBO technique over DTBO, ODTBO in terms of convergence rate and best-possible solution. Moreover, by doing statistical analysis on IEEE CEC 2017 benchmark functions, the robustness of the suggested CODTBO optimization technique has been assessed.

Keywords Combined heat and power economic dispatch (CHPED) · Optimal power flow (OPF) · IEEE-57 bus · Wind energy · Solar energy · Electrical vehicle (EV) · Driving training based optimization (DTBO) · Chaotic-oppositional based DTBO (CODTBO)

List of symbols

V_{wind}	Wind initial velocity
$k > 0$	Shape factor
CDF	Cumulative density function
P_{wrated}	Rated wind power
V_{in}	Cut-in wind velocity
$\text{TotalCost}_{\text{wind}}$	Total wind cost
$\text{Cost}^{\text{O}}_{\text{windm}}$	Overestimation wind cost
$\text{Pf}^{\text{U}}_{\text{windm}}$	Underestimation wind cost coefficient
i_{rd}	Solar irradiance
S	Output solar power
R_{C}	Specific irradiance point
P_{solaravl}	Average power

✉ Chandan Paul
chandan815@rediffmail.com

[1] Department of Electrical Engineering, Dr. B. C. Roy Engineering College, Durgapur, India

[2] Department of Electrical Engineering, Kalyani Government Engineering College, Kalyani, West Bengal, India

Published online: 30 January 2024

P_{srl}	Rated solar power
N_l	Number of vehicles
$E_{\text{EV},t}$	Power to charge
$\text{soc}_{\text{initial}}$	Initial value of state of charging
η_{charging}	Charging efficiency
$E_{\text{EV},q}^{\text{driving}}$	Driving power of vehicle
m	Mean
d_l^{EV}	Direct cost coefficients
$Gf\ (*)$	Function of Gauss error
$\text{PF}_{\text{EVl}}^{\text{U}}$	Underestimated penalty factor of EV
$\text{Cost}_{\text{poui}}\left(P_{\text{poui}}\right)$	Fuel cost of the power generator
$\text{Cost}_{\text{houi}}\ (H_{\text{houi}})$	Generation cost of heat
N_{pou}	Number of power units
N_{hou}	Number of heat units
δ_{poui} and $\varepsilon_{\text{poui}}$	Valve point coefficients
$\text{Cost}_{\text{windi}}\ (P_{\text{windi}})$	Wind generation cost
$P_{\text{poui}}^{\text{t}}$	Thermal power output
N_{L}	Total number of transmission line
ϵ_1, ϵ_2	Penalty factor
P_{Lc}	Active power demand of cth bus
Y_{cd}	Admittance of transmission line
$P_{\text{poui}}^{\min}, P_{\text{poui}}^{\max}$	Minimum and maximum power limits
$P_{\text{windi}}^{\min}, P_{\text{windi}}^{\max}$	Wind minimum and maximum power
$V_{\text{Gb}}^{\min}, V_{\text{Gb}}^{\max}$	Lower and upper voltage limits
$Q_{\text{Gb}}^{\min}, Q_{\text{Gb}}^{\max}$	Minimum and maximum reactive power
${S_{\text{Lb}}}^{\min},\ S_{\text{Lb}}^{\max}$	Minimum and maximum apparent power
Z_p pth	Member of the population
Z_p^{st2}	Modified pth candidate solution
a and b	Minimum and maximum limits of search space's
$j_{\text{R,Min}}, j_{\text{R,Max}}$	Minimum and maximum jumping rate
f_{Max}	Maximum iteration
ran	Random value
$d > 0$	Scale factor
P_{wind}	wind output power
V_{rated}	Rated wind velocity
V_{out}	Cut-out wind velocity
N_{wind}	Total number of wind units
$\text{Cost}_{\text{windm}}^{\text{U}}$	Underestimation wind cost
$\text{Pf}_{\text{windm}}^{\text{O}}$	Overestimation wind cost coefficient
S_{R}	Rated solar power
$i_{\text{rd,sd}}$	Solar standard irradiance
P_{solarshl}	Scheduled solar power
$\text{PF}_{\text{solarl}}^{\text{O}}$	Penalty cost coefficient
$\text{PF}_{\text{sl}}^{\text{U}}$	Penalty cost coefficient
I	Fleet index
SOC	State of charging
C_{EV}	Capacity of EV battery
$\eta_{\text{discharging}}$	discharging efficiency
$f_{P_{\text{EV}}}\ (P_{\text{EV}})$	PDF power output of EV
σ	standard deviation
P_{EVshl}	scheduled power of EV
P_{EVl}	output power
$\text{PF}_{\text{EVl}}^{\text{O}}$	Overestimated panalty factor
$\text{Cost}_{\text{ci}}\left(P_{\text{chpi}},\ H_{\text{chpi}}\right)$	Generation cost of co-generation
P_{poui}	Power of ith unit
N_{chp}	Number of CHP units
α_{poui}, β_{poui} and γ_{poui}	Coefficients of thermal units
$\text{Cost}_{\text{windi}}\ (P_{\text{windi}})$	Wind generation cost
$b_{i0}, b_{i1}, b_{i2}, b_{i3}$ and b_{i4}	Emission coefficients
$G_{n(pq)}$	Transfer conductance of nth line
ϕ_{pq}	voltage angle between buses p and q
H_D and B_{im}, B_{ij}, B_{jr}	Power loss coefficients
Q_{Lc}	Reactive power demand of cth bus
φ_{cd}	Admittance angle of transmission line
$P_{\text{chpi}}^{\min}\left(H_{\text{chpi}}\right), P_{\text{chpi}}^{\max}\left(H_{\text{chpi}}\right)$	Minimum and maximum power
$H_{\text{chpi}}^{\min}, H_{\text{chpi}}^{\max}$	Minimum and maximum heat
$P_{\text{Gb}}^{\min}, P_{\text{Gb}}^{\max}$	Lower and upper bounds
$V_{\text{Lb}}^{\min}, V_{\text{Lb}}^{\max}$	Smallest and highest voltage edges
bth	Transformer
N	Population size
ξ	Patterning index
j_{R}	Jumping rate
f	Function for current iteration
t	Time index

1 Introduction

At all thermal power plants, heat is discharged into the environment during the production of electricity, either by flue gas, cooling towers, or another method. Because of the byproducts produced during heating, such as NOX, SOX, SO_2, and CO_2, the power developing units' energy efficiency plummets to an extremely poor value (between 50% and 60%), and the environment is subsequently polluted. In the field of power system research, issues with combined heat and power economic dispatch (CHPED) are crucial. The amount of pollutants emitted into the atmosphere is

reduced and manufacturing costs are decreased by using the waste heat from the steam. In CHPED, the heat recovery steam generator uses chillers to recover the heat lost during the production of steam and cooling. The CHPED is a co-generation system that concurrently generates heat and electricity. Despite requiring additional capital, CHPED boosts thermal generating station efficiency to above 75%.

The CHPED mainly focused on economic power generation not on the power flow of transmission line. In power systems, optimal power flow (OPF) is a well-researched optimization issue. Carpentier [2] originally presented this issue in 1962. Finding a steady-state operating point (OPF) that satisfies operating limitations and meets demand while reducing the cost of electric power generation is the goal of OPF. So, it is required to coupled CHPED with OPF to address the need for affordable power generation with optimized power flow in transmission lines. Researchers studying electrical power systems have been concentrating on finding various optimization strategies to solve the optimal power flow (OPF) problem during the past few decades. OPF strives to find a solution that is workable from various critical elements including economics, the environment, dependability, security, and power quality, among others, while keeping in mind all of the various power system constraints.

Researchers were employed in the early stages of OPF problems to attain the lowest fuel cost, using thermal generators as the only option. However, as time goes on, a number of circumstances, including increasing power consumption, environmental regulations, the depletion of fossil fuels, the need for a carbon price, etc., force the integration of an increasing number of renewable energy sources into the existing power networks. Trying to use unconventional energy sources undoubtedly makes the network much more difficult. Numerous evolutionary techniques have been applied in the literature to address the severely non-convex and nonlinear OPF problem. By adjusting the generators' schedules, terminal voltages, tap settings, and VAR compensation, it is possible to minimize the cost of generation, active power loss, fuel emission, and voltage deviation while still meeting network capability, generator capacity, network security, and power balance constraints.

1.1 Literature review

During the last two decades various researchers have presented lots of research on single- and multi-objective functions using different optimization techniques with satisfying all constraints. Different classical techniques had been tested on CHPED and OPF including the Lagrangian relaxation (LR) [1], the statistical process control method [2], linear programming [3], nonlinear programming [4] and quadratic programming [5]. Since classical approaches are based on differential calculus and numerical methods, they are unable to handle non-differentiable and nonlinear functions. In order to resolve the local optimum problem of nonlinear-based difficulties, several authors applied various evolutionary-based optimisation methodologies to arrive at the global optimal solution. In order to find the best solution, Paul et al. [6] used the whale optimisation approach (WOA) to take nonlinearities such valve point loading (VL) and the banned operating zone (POZ) of thermal units into consideration. Betar et al. [7] recommended hybrid Harris Hawks for the economic load dispatch (ELD) problem with notable performances. To evaluate the effectiveness of the proposed algorithm on a real-world base system,

Dutta et al. [8] utilized chemical reaction optimization technique (CRO) to find the optimal location of UPFC for economic power generation with maintained the constraints of power system of OPF problem. Roy and Paul [9] illustrated the krill heard algorithm (KHA) to evaluate the superiority of the KHA approach on the OPF problem. The KHA approach was tested on several IEEE bus systems, and comparisons were performed with alternative optimization strategies. Shahhen et al. [10] implemented heap-based optimization on different buses of integrated feeder-based distribution generator for OPF with various objective functions. Fergany and Hasanien [11] tested tree seed algorithm on different buses with various multi-objective functions with optimal flow through transmission lines. Xiao et al. [12] suggested meta-model-based optimization technique to investigate the superiority of the applied method on OPF. Mukherjee et al. [13] proposed krill heard algorithm (KHA) to solve the OPF problem with considering the constraint of transient stability which helps to simultaneously balanced cost and dynamic stability. Mandal et al. [14] recommended TLBO optimization technique incorporated with quasi-oppositional-based learning to obtain global optimal solution for OPF problem of different single- and multi-objective functions.

In the present scenario fuel is improvising day by day, so it is an important aspect use of renewable energy sources for economic power generation. Lots of researchers used the renewable energy sources with conventional power generating units to reduce the use of fuel for economic power generation. Hazra and Roy [15] recommended moth flame optimization (MFO) on HTS problem integrated with renewable energy for economic and emission less operation. Paul et al. [16] tested WOA incorporated with chaotic-based learning (CWOA) on two test systems of CHPED problem with consideration of wind energy source for economic power generation. Paul et al. [17] suggested quasi-oppositional-based learning WOA (QOWOA) on CHPED system with considering the VL and POZ and to reduce the use of thermal power unit renewable energy sources also incorporated with the CHPED problem. Further, chaotic-based learning is combined with QOWOA (CQOWOA) by Paul et al. [18] to achieve the best results in order to deal with increased

nonlinearity brought on by the increased number of non-conventional energy sources with CHPED system.

Zhang et al. [19] proposed the gradient tracking optimization technique to study the short-term OPF problem on IEEE 39 bus and 118 bus system with taking into account the wind power generation to accomplish the realistic optimization control. Evangeline and Rathika [20] presented the horse herd algorithm (HHA) for the multi-objective OPF problem to obtain the best results in terms of economic operation and reducing green house effect. concentrated on regulating voltage deviation and transmission losses as well for ideal power flow in the transmission line. The system incorporates wind power generation, which reduced fuel usage and emissions. For the IEEE-30 and 57 bus OPF challenge, Li et al. [21] incorporated non-conventional energy sources with the suggested solution. Weibull and lognormal PDF have been used to reduce the uncertainty of wind speed and solar intensity. For the 39-bus system, Chen et al. [22] suggested semidefine programming (SDP) to handle the effect of renewable energy sources on the OPF problem while taking into account transient stability limitations. Sulaiman et al. [23] presented teaching-learning-based optimization (TLBO) on the wind–solar-based OPF issue to get the best response for single and multi-objective cost and emission functions. Basu [24]suggested elephant clan optimization (ECO) for renewable-based dynamic OPF problem on different IEEE buses and 15 bus micro-grid for validation of the proposed technique over cost minimization.

Naderi et al. [25] implemented shuffled frog leaping algorithm (SFLA) on OPF problem to solve multi-objective functions where FACTS devices have been used to get optimal solution over cost, emission, transmission losses and voltage deviation. In [26], Naderi et al. analyzed optimal active power dispatch (OAPD) problem integrated with FACTS devices to obtain optimal solution over cost minimization using hybrid fuzzy-based technique. Furthermore, Naderi et al. [27] proposed self-adaptive approach for solving OPF problem on IEEE 30-, 57- 118-bus for optimal solution. Alizadeh et al. in their recent endeavor proposed transactive control approach in microgrid [28] for energy governing policy using different renewable energy sources. Recently, He et al. [29] utilized FACTS devices on renewable energy-based integrated power system to improve the stability by suppressing the low order frequency using PSO-GA-based optimization technique. Kumar and Sharma [30] in their recent work, introduced FOPID-PR controller to improve the stability of the power system by controlling frequency and power deviation during disturbances.

1.2 Research gaps of the existing algorithms

After thorough literature survey, the merits and demerits of different optimization algorithms used in different power system area for solving single and multi-objective functions to obtain effective solution of are summarized and displayed in Table 1. It has been observed from Table 1 that most of the existing optimization techniques suffer from local optima problem, sensitive to initial population, poor convergence rate, less accuracy, inability to deal with high dimensional problem. The limitation of the existing techniques is overcome by integrating chaotic-opposition-(CO) based learning approach with DTBO (CODTBO). The CO learning enhances the searching ability of the proposed approach which tunes the coefficient of the control variable to reach the optimal solution.

1.3 Motivation and incitement

This article throws light on the following motivating factors of research

(a) Improvising of the fossil fuels in the present scenario.
(b) Environmental concerns resulting in the implementation of incentive measures to reduce the pollution from fossil fuels.
(c) For energy utilities, balancing supply and demand effectively and economically has become a challenge task due to the increase in electricity demand.
(d) Importance of combined scheduling of thermal generating unit with renewable energy sources.
(e) Presence of nonlinearity namely, uncertainty of wind speed, solar irradiation and PEV uncertainties etc. of the renewable energy sources.
(f) The above literature review reveals that there are still some gaps in the research work. Most of these optimization techniques suffer from local optima problems, less convergence speed and are taking more computational time resulting in unsatisfactory outcomes.

1.4 Contribution

The main contributions of the paper are as follows:

(a) In the proposed work, optimal power flow (OPF)-based combined heat and power economic dispatch (CHPED) which is a new approach in the present scenario, is successfully introduced to supply electric power with maintaining the permissible load bus voltage.
(b) Secondly, to reduce the fuel consumption in the thermal power plant, the renewable energy sources like wind, solar and electric vehicle have been integrated with OPF-based CHPED system which is not attempted earlier in the existing research works. The scheduling model of IEEE 57-bus system is displayed in Fig. 1.
(c) From the literature review it has been observed that existing optimization techniques have several limita-

Table 1 Literature review of the existing algorithms

Name	Classifications	Mechanisms	Merits	Demerits
LR [1]	Classical technique	Iterative optimization	Many ways to obtain feasibility	Computationally expensive, sensitive in choice of control parameters
SP [2]	Classical technique	Based on statistical evidences	Better accuracy	Complexity, scalability and decomposition
LP [3]	Classical technique	Mathematical model	Better resource allocation, streamlined decision-making	Assumption on linearity, errors sensitivity
NP [4]	Classical method	Objective functions are non-linear based	Better flexibility and accuracy	More memory required
QP [5]	Classical method	Nonlinear programming	Simple for equality constraints problem	More simulation time and complex
WOA [6]	Evolutionary algorithm	Encircling prey, Bubble-net attacking technique of humpback whales	Can overcome local optima	Slow convergence speed
HHHA [7]	Evolutionary algorithm	Population and nature based	Strong robustness	Premature convergence
CRO [8]	Evolutionary algorithm	Chemical reaction based	Greater flexibility	Not applicable for large scale problem
KHA [9]	Evolutionary algorithm	Crossover and mutation operation	Provide optimal solution	Less convergence rate
HBO [10]	Evolutionary algorithm	Tree based data structure	Efficient in shorting	Less flexibility
TSA [11]	Evolutionary algorithm	Based on trees and seeds	High accuracy	More computing time
MMBO [12]	Evolutionary algorithm	Based on surrogate model	Higher efficiency	Less accuracy
TLBO [14]	Evolutionary algorithm	Population based, teaching-learning	Less parameters required	Poor population diversity
MFO [15]	Evolutionary algorithm	Transverse orientation	Fast converging	Sensitive in initial population
CWOA [16]	Evolutionary algorithm	Based on encirclement prey and bubble net searching	Can overcome local optima	Better convergence speed than WOA.
QOWOA [17]	Evolutionary algorithm	Based on encirclement prey and bubble net searching	Can overcome local optima	Better convergence speed than WOA.
CQOWOA [18]	Evolutionary algorithm	Based on encirclement prey and bubble net searching	Can overcome local optima	Better convergence speed than QOWOA.
GTO [19]	Evolutionary algorithm	Based on gradient descent	Needs more memory	Better convergence speed.
HHA [20]	Evolutionary algorithm	Nature based	More accuracy	More time for mutation
SDP [22]	Evolutionary algorithm	Linear programming based	More powerful	More complex
ECO [24]	Evolutionary algorithm	Based on elephant behavior	Avoid local optima	Slow convergence
SFLA [25]	Evolutionary algorithm	Based on quantum rotation angle	Global optimization ability	Slow convergence
FF [26]	Evolutionary algorithm	Based on set theory	Easy and understandable	Always not accurate
TCA [28]	Evolutionary algorithm	Based on decentralized decision making	Transparent characteristics	Complex

tions. To overcome the existing research gaps, a newly developed driving-training-based-optimization (DTBO) technique and its improved version namely, chaotic-oppositional-based DTBO (CODTBO) have been tested on the proposed systems to obtain the best possible solution for the power system.

(d) Different single objective functions like cost minimization, emission minimization, voltage stability minimization and various multi-objective functions like cost with emission and cost with voltage stability have been discussed .

(e) Statistical analysis has been performed to judge the robustness of the proposed optimization technique.

1.5 Limitation of the proposed technique

In this research work, the suggested algorithm is not carried out on a real-time environment.

1.6 Paper organization

Here is how the remainder of the paper is organized: Sect. 2 includes the details of wind, solar and electric vehicle (EV) for power generation. In Sect. 3, the proposed system's problem formulation is shown. The different steps of proposed optimization technique with flowchart has been discussed in Sect. 4. Implementation of the proposed technique in solving benchmark functions and OPF-based CHPED have been illustrated in Sect. 4. Section 6 of the proposed system reports its conclusion.

2 Details of wind power

Due to its reliance on wind speed, which results in lower production costs and zero emissions. As wind power cannot meet the entire demand for electricity, it is preferable to connect it to other sources of power to create a stable supply. The power dispatch to the grid is impacted by the wind power uncertainty, which is explored further below.

2.1 Wind power uncertainty functions

The term "dispatchable energy sources of electricity" describes those sources that can produce electricity when it is needed. But what makes it challenging to integrate the wind units with the grid is the uncertainty of wind sources caused by wind speed. The Weibull PDF is frequently used to depict wind speed, as demonstrated in (1).

$$F_{\text{rand}}(V_{\text{wind}}) = \frac{k}{d}\left(\frac{V_{\text{wind}}}{d}\right)^{k-1} \times e^{-\left(\frac{V_{\text{wind}}}{d}\right)^{k}} \tag{1}$$

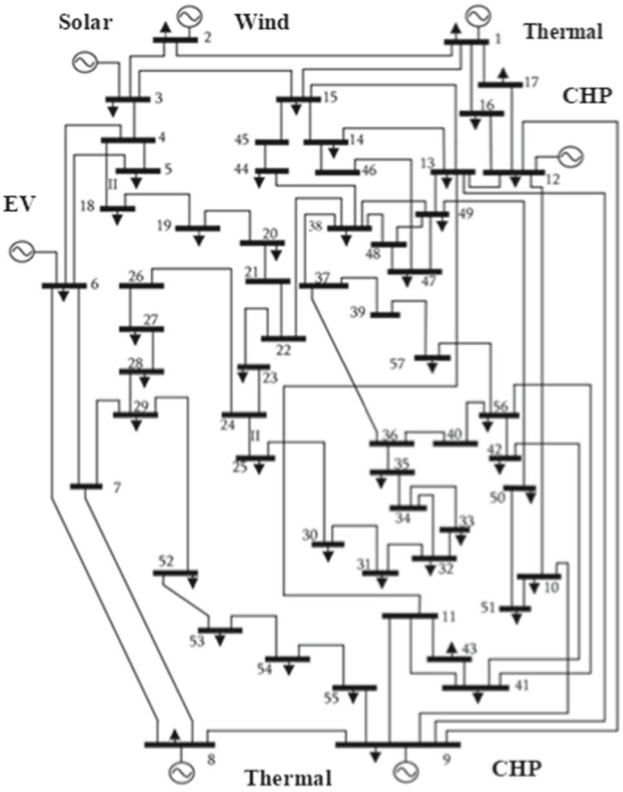

Fig. 1 The single line diagram of the IEEE-57 bus system with Thermal-CHP-wind–solar–EV

where initial velocity of wind defined by V_{wind}; random value signifies with ran; $k > 0$ denotes the shape factor whereas $d > 0$ signifies scale factor. A representation of the cumulative density function (CDF) is shown in Fig. 2.

$$f_{\text{rand}}(V_{\text{wind}}) = 1 - e^{-\left(\frac{V_{\text{wind}}}{d}\right)^{k}} \tag{2}$$

Several researchers have assessed a linear model to estimate wind power (see (3)) by utilizing wind velocity.

$$P_{\text{wind}} = \begin{cases} 0 & V_{\text{wind}} < V_{\text{in}} \; or \; V_{\text{wind}} > V_{\text{out}} \\ \frac{P_{\text{wrated}}(V_{\text{wind}} - V_{in})}{V_{\text{rated}} - V_{in}} & V_{\text{in}} \le V_{\text{wind}} < V_{\text{rated}} \\ P_{\text{wrated}} & V_{\text{rated}} \le V_{\text{wind}} < V_{\text{out}} \end{cases} \tag{3}$$

where P_{wind} and P_{wrated} are signify the wind output power and rated power; rated wind velocity denotes with V_{rated}; cut-in and cut-out velocity of wind represent with V_{in} and V_{out}; representation of PDF of P_{wind} illustrated in (4).

$$F_{P_{\text{wind}}}(P_{\text{wind}}) = \frac{ku}{dP_{\text{wrated}}}\left(\frac{V_{\text{in}} + u\frac{P_{\text{wind}}}{P_{\text{wrated}}}}{d}\right)^{k-1} \times e^{-\left(\frac{V_{\text{in}} + u\frac{P_{\text{wind}}}{P_{\text{wrated}}}}{d}\right)^{k}} \tag{4}$$

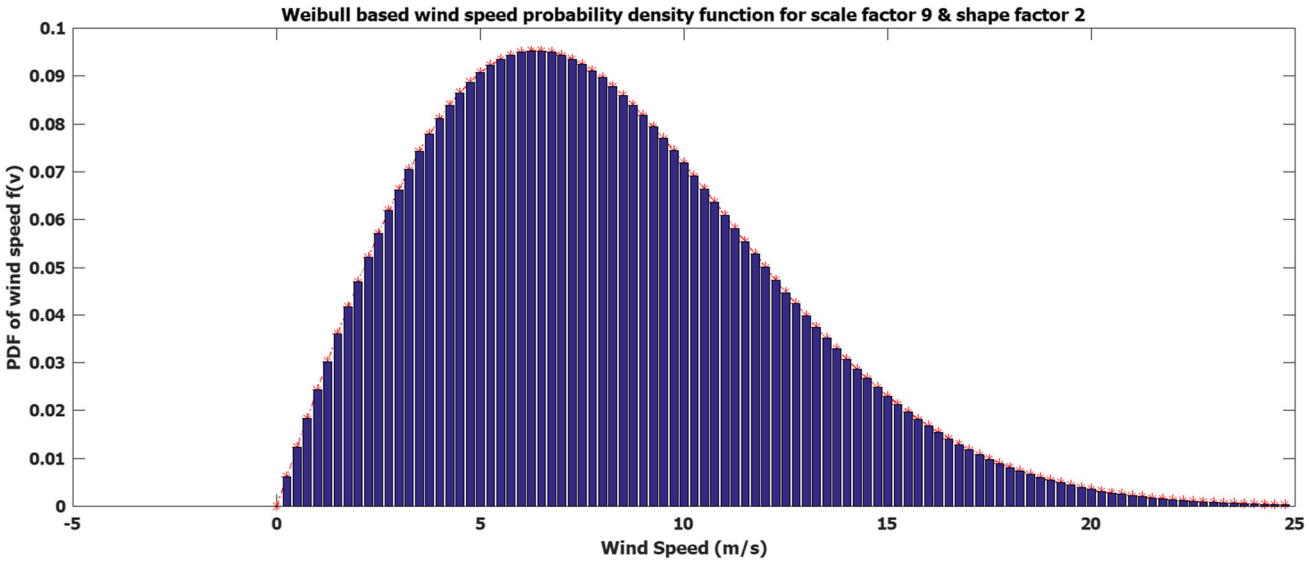

Fig. 2 Weibul based wind velocity PDF

where $u = V_{\text{rated}} - V_{\text{in}}$

The two discrete probabilities when P_{wind} equals 0 or P_{wrated}, the continuous probability is represented as follows:

$$\begin{cases} S_{\text{rated}}\left(P_{\text{wind}}=0\right) = S_{\text{rated}}\left(V < V_{\text{in}}\right) + S_{\text{rated}}\left(V > V_{\text{out}}\right) \\ \quad = 1 - e^{-\left(\frac{V_{\text{in}}}{d}\right)^{k}} + e^{-\left(\frac{V_{\text{out}}}{d}\right)^{k}} \end{cases} \tag{5}$$

$$\begin{cases} S_{\text{rated}}\left(P_{\text{wind}}=P_{\text{wrated}}\right) = S_{\text{rated}}\left(V_{\text{rated}} \le V < V_{\text{out}}\right) \\ \quad = e^{-\left(\frac{V_{\text{rated}}}{d}\right)^{k}} - e^{-\left(\frac{V_{\text{out}}}{d}\right)^{k}} \end{cases} \tag{6}$$

CDF of P_{wind} is obtained by integrating Eqs. (5) and (6), which is illustrated in (7).

$$f_{P_{\text{wind}}}\left(P_{\text{wind}}\right) = \begin{cases} 0 & Pwind < 0 \\ \frac{ku}{dP_{\text{wrated}}}\left(\frac{V_{\text{in}}+u\frac{P_{\text{wind}}}{P_{\text{wrated}}}}{d}\right)^{k-1} \times e^{-\left(\frac{V_{\text{in}}+u\frac{P_{\text{wind}}}{P_{\text{wrated}}}}{d}\right)^{k}} & 0 \le P_{\text{wind}} < P_{\text{wrated}} \\ 1 & P_{\text{wind}} \ge P_{\text{wrated}} \end{cases} \tag{7}$$

2.2 Determination of wind cost.

The unpredictability of the wind will affect when to schedule wind power generating units into the system during times of peak load. Uncertainty in electricity generation is brought on by the unpredictable nature of the wind speed along the coast. Weibull's probability density function shown in Fig. 2 will be used to examine the anticipated uncertainty costs associated with wind energy. Overestimation and underestimation serve as definitions for this function (8).

$$\begin{cases} \text{TotalCost}_{\text{wind}} = \sum_{m=1}^{N_{\text{wind}}} \text{Cost}_{\text{windm}}\left(P_{\text{windm}}\right) \\ = \sum_{m=1}^{N_{\text{wind}}} \left(\text{Cost}^{\text{O}}_{\text{windm}} + \text{Cost}^{\text{U}}_{\text{windm}}\right) \end{cases} \tag{8}$$

where $\text{TotalCost}_{\text{wind}}$ represents the total wind cost and N_{wind} denotes the total number of wind units.

2.2.1 Wind overestimation cost calculation

When the actual power is lower than the intended generated power, the cost of overestimation is described. This indicates that the wind-generated power will not be sufficient to meet the load requirement. The excess power needed to meet the load demand will be supplied by the spinning reserve. The cost of overestimation can be calculated from (9).

$$\begin{cases} \mathrm{Cost}^{\mathrm{O}}_{\mathrm{windm}} = \mathrm{Pf}^{\mathrm{O}}_{\mathrm{windm}} \times P_{\mathrm{windm}} \\ \left[1 - e^{-\left(\frac{V_{\mathrm{in}}}{s}\right)^{j}} + e^{-\left(\frac{V_{\mathrm{out}}}{s}\right)^{j}}\right] + \\ \left(\frac{P_{\mathrm{wratedm}} V_{\mathrm{in}}}{V_{\mathrm{rated}} - V_{\mathrm{in}}} + P_{\mathrm{windm}}\right) \\ \left[e^{-\left(\frac{V_{\mathrm{in}}}{c}\right)^{j}} - e^{-\left(\frac{V_{\mathrm{in}} + P_{\mathrm{windm}} \frac{V_{\mathrm{rated}} - V_{\mathrm{in}}}{P_{\mathrm{wrated}}}}{s}\right)^{j}}\right] \\ + \left(\frac{P_{\mathrm{wrated}} s}{V_{\mathrm{rated}} - V_{\mathrm{in}}}\right)\left[\zeta\left\{1 + \frac{1}{j}, \left(\frac{V_{\mathrm{in}} + P_{\mathrm{windm}} \frac{V_{\mathrm{rated}} - V_{\mathrm{in}}}{P_{\mathrm{wrated}}}}{s}\right)^{j}\right\}\right. \\ \left. -\zeta\left\{1 + \frac{1}{j}, \left(\frac{V_{\mathrm{in}}}{s}\right)^{j}\right\}\right] \end{cases} \tag{9}$$

2.2.2 Wind underestimation cost calculation

Underestimation costs are incurred when actual wind energy is greater than anticipated. Batteries will be used to store any additional electrical energy generated by wind turbines since otherwise it will be lost of generated power. The formulation to calculate the underestimation cost is represented as below (10):

$$\begin{cases} \mathrm{Cost}^{\mathrm{U}}_{\mathrm{windm}} = \mathrm{Pf}^{\mathrm{U}}_{\mathrm{windm}} \times (P_{\mathrm{wrated}} - P_{\mathrm{windm}}) \\ \left[e^{-\left(\frac{V_{\mathrm{rated}}}{s}\right)^{j}} - e^{-\left(\frac{V_{\mathrm{out}}}{s}\right)^{j}}\right] + \\ \left(\frac{P_{\mathrm{wrated}} V_{\mathrm{in}}}{V_{\mathrm{rated}} - V_{\mathrm{in}}} + P_{\mathrm{windm}}\right) \\ \left[e^{-\left(\frac{v_{\mathrm{rated}}}{s}\right)^{j}} - e^{-\left(\frac{V_{\mathrm{in}} + P_{\mathrm{windm}} \frac{v_{\mathrm{rated}} - v_{\mathrm{in}}}{P_{\mathrm{wrated}}}}{s}\right)^{j}}\right] \\ + \frac{P_{\mathrm{wrated}} s}{V_{\mathrm{rated}} - V_{\mathrm{in}}}\left[\zeta\left\{1 + \frac{1}{j}, \left(\frac{V_{\mathrm{in}} + P_{\mathrm{windm}} \frac{V_{\mathrm{rated}} - V_{\mathrm{in}}}{P_{\mathrm{wrated}}}}{s}\right)^{j}\right\}\right. \\ \left. -\zeta\left\{1 + \frac{1}{j}, \left(\frac{V_{\mathrm{rated}}}{s}\right)^{j}\right\}\right] \end{cases} \tag{10}$$

In the above equations overestimation and underestimation cost of mth wind unit signified with $\mathrm{Cost}^{\mathrm{O}}_{\mathrm{windm}}$ and $\mathrm{Cost}^{\mathrm{U}}_{\mathrm{windm}}$; rated output power and rated velocity denoted by P_{wrated} and V_{rated}; V_{in} and V_{out} are cut-in and cut-out velocity of wind; $\mathrm{Pf}^{\mathrm{U}}_{\mathrm{windm}}$ is underestimation and $\mathrm{Pf}^{\mathrm{O}}_{\mathrm{windm}}$ is overestimation cost co-efficient, respectively.

2.3 Details of solar power

The lognormal-based solar irradiance-based probability distribution function is displayed in Fig. 3. The following Eq. (11) shows the generation of solar power due to solar irradiance i_{rd}.

$$f_{\mathrm{solar}}(i_{\mathrm{rd}}) = \frac{1}{i_{\mathrm{rd}} d\sqrt{2\pi}} e^{\frac{-(\ln i_{\mathrm{rd}} - M)^2}{(2d)^2}} \quad \text{for} \quad i_{\mathrm{rd}} > 0 \tag{11}$$

Below is an expression of the power output of a solar unit as a function of i_{rd}.

$$\begin{cases} P_{\mathrm{solar}} = P_{\mathrm{sr}}\left(\frac{{i_{\mathrm{rd}}}^2}{i_{\mathrm{rd,sd}} R_{\mathrm{C}}}\right) & for \quad 0 < i_{\mathrm{rd}} < R_{\mathrm{C}} \\ \quad = P_{\mathrm{sr}}\left(\frac{i_{\mathrm{rd}}}{i_{\mathrm{rd,sd}}}\right) & \text{for} \quad i_{\mathrm{rd}} > R_C \end{cases} \tag{12}$$

where S_{R} and S are the rated and output power of solar unit; solar standard irradiance and specific irradiance point are signifies with $i_{\mathrm{rd,sd}}$ (=1000 w/m^2) and R_{C} (= 150 w/m^2).

2.3.1 Solar cost calculation

The cost of electricity production for a solar unit is computed using the sum of three different cost functions, which are as follows [31]:

$$\mathrm{Cost}_{\mathrm{solarl}}(P_{\mathrm{solarl}}) = \mathrm{Cost}^{\mathrm{d}}_{\mathrm{solarl}} + \mathrm{Cost}^{\mathrm{O}}_{\mathrm{solarl}} + \mathrm{Cost}^{\mathrm{U}}_{\mathrm{solarl}} \tag{13}$$

In the above equation direct cost, overestimation cost and underestimation cost are denoted with $\mathrm{Cost}^{\mathrm{d}}_{\mathrm{solarl}}$, $\mathrm{Cost}^{\mathrm{O}}_{\mathrm{solarl}}$ and $\mathrm{Cost}^{\mathrm{U}}_{\mathrm{solarl}}$ of the lth solar unit.

2.3.1.1. Solar direct cost: Direct costs are the costs incurred during the production of solar energy. If the system operator owns the solar farm, this sentence is absent. The equation below provides the solar energy's direct cost.

$$\mathrm{Cost}^{\mathrm{d}}_{\mathrm{solarl}} = d_l^{\mathrm{solar}} P_{\mathrm{solarshl}}, \quad \text{where} \quad l = 1, 2, 3.., n_{\mathrm{s}} \tag{14}$$

Here, d_l^{s} represents direct cost coefficients and P_{solarshl} and schedule power of the lth solar.

2.3.1.2. Solar overestimation cost: If the amount of solar power available is less than what is scheduled, the overestimation cost is calculated using the formula below.

$$\begin{cases} \mathrm{Cost}^{\mathrm{O}}_{\mathrm{solarl}} = \mathrm{PF}^{\mathrm{O}}_{\mathrm{solarl}}(P_{\mathrm{solarshl}} - P_{\mathrm{solaravl}}) \\ \quad = \mathrm{PF}^{\mathrm{O}}_{\mathrm{solarl}} \int_{0}^{P_{\mathrm{vsolarshl}}} (P_{\mathrm{solarshl}} - P_{\mathrm{solar}}) \\ \quad \times f_{P_{\mathrm{solar}}}(P_{\mathrm{solar}})\, \mathrm{d}P_{\mathrm{solar}} \end{cases} \tag{15}$$

where PDF of the power output of solar unit signifies with $f_{p_{\mathrm{s}}}(P_{\mathrm{solar}})$; P_{solarshl}, P_{solaravl} and $\mathrm{PF}^{\mathrm{O}}_{\mathrm{solarl}}$ are the scheduled power, average power and overestimation penalty cost coefficient of the lth solar unit.

2.3.1.3. Solar underestimation cost: The underestimating cost of the lth solar unit is determined as follows if the solar power that is available is greater than the power that is sched-

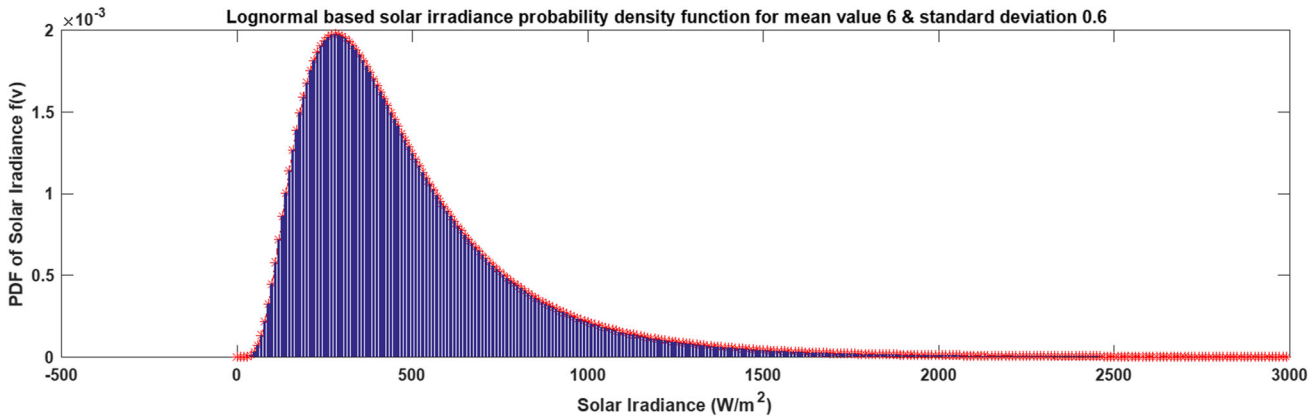

Fig. 3 Weibul-based wind velocity PDF

uled.

$$\begin{cases} \text{Cost}^{\text{U}}_{\text{solarl}} = \text{PF}^{\text{U}}_{\text{solarl}} \left(P_{\text{solaravl}} - P_{\text{solarshl}}\right) \\ \quad = PF^{\text{U}}_{\text{solarl}} \int_{P_{\text{solarshl}}}^{P_{\text{solarrl}}} \left(P_{\text{s}} - P_{\text{solarshl}}\right) \\ \quad \times f_{p_{\text{s}}}\left(P_{\text{solar}}\right) \text{d}P_{\text{Solar}} \end{cases} \tag{16}$$

where P_{srl} and $\text{PF}^{\text{U}}_{\text{sl}}$ are the rated power and underestimation panalty cost coefficient of the lth solar unit.

2.4 Details of EVs

Electric vehicles (EVs) consume electricity from the grid during the valley load period and provide electricity for the grid at peak load. The amount of time that EVs spend charging, discharging, and driving can be used to represent the entirety of a 24-h period. The following two equations illustrate how EVs express their charging and discharging power.

$$P^{\text{charge}}_{I,t} = -\sum_{v=1}^{N_l} \text{Minimum}\left(0, E_{\text{EV},t}\right) \tag{17}$$

$$P^{\text{discharge}}_{I,t} = \sum_{v=1}^{N_l} \text{Maximum}\left(0, E_{\text{EV},t}\right) \tag{18}$$

The fleet size is reflected by the number of vehicles N_l; representation of the electrical vehicle fleet index is I; t is the time index; $E_{\text{EV},t}$ represents the EVs' power to charge and discharge to the grid.

The state of charge in relation to the battery's capacity, or SOC, is what allows an electric motor to accelerate a vehicle. In addition to preventing battery losses, SOC safeguards the battery from excessive charging and draining. The SOC of EV is depicted as follows.

$$\begin{cases} \text{SOC}_{\text{EV},t} = \text{SOC}_{\text{init}} - \frac{1}{C_{\text{EV}}} \sum_{q=1}^{t} \\ \left[\text{Minimum}\left(0, E_{\text{EV},q}\right) \times \eta_{\text{charging}}\right] - \frac{1}{C_{\text{EV}}} \sum_{q=1}^{t} \\ \left[\text{Maximum}\left(0, E_{\text{EV},q}\right) \times \eta_{\text{discharging}} + E^{\text{drv}}_{\text{EV},q}\right] \end{cases} \tag{19}$$

The SOC of EV at time t is represented by $\text{soc}_{\text{EV},t}$; initial value of state of charging is denoted by $\text{soc}_{\text{initial}}$; C_{EV} signifies the capacity of EV battery. In EV, battery η_{charging} and $\eta_{\text{discharging}}$ signify charging and discharging efficiency; driving power of vehicle at q_{th} time is denoted by $E^{\text{driving}}_{\text{EV},q}$.

2.4.1 Stochastic model of EVs

This study suggests using a stochastic model of EVs to calculate their potential energy storage capacity. With the following PDF, V2G power exhibits a normal distribution:

$$f_{P_{\text{EV}}}\left(P_{\text{EV}}\right) = \frac{1}{\sqrt{2\pi\sigma^2}} e^{-\left(P_{\text{EV}}-m\right)^2 / 2\sigma^2} \tag{20}$$

where $f_{P_{\text{EV}}}\left(P_{\text{EV}}\right)$ corresponds the PDF of the power output of EV unit; m is mean and σ is standard deviation of the normal distribution function.

2.4.2 Electric vehicle (EV) cost calculation:

For the lth EV unit, there are three costs associated with using electric vehicles. and it is formulated as follows:

$$\text{Cost}_{\text{EVl}}\left(P_{\text{EVl}}\right) = \text{Cost}^{\text{d}}_{\text{EVl}} + \text{Cost}^{\text{O}}_{\text{EVl}} + \text{Cost}^{\text{U}}_{\text{EVl}} \tag{21}$$

where $\text{Cost}^{\text{d}}_{\text{EVl}}$, $\text{Cost}^{\text{O}}_{\text{EVl}}$ and $\text{Cost}^{\text{U}}_{\text{EVl}}$ are the direct cost, the overestimation cost and the underestimation cost of the lth EV unit, respectively.

2.4.2.1. EV direct cost: The direct cost of lth EV unit may be computed as follows:

$$\text{Cost}^{\text{d}}_{\text{EVl}} = d_l^{\text{EV}} P_{\text{EVshl}}, \quad \text{where} \quad l = 1, 2, 3.., n_v \tag{22}$$

where d_l^{EV} implies direct cost coefficients for the lth EV unit; n_{EV} is the number of EV units; P_{EVshl} is the scheduled power of the lth EV unit.

When the available EV power is greater than the intended power, the miscalculation cost becomes apparent. The underestimate penalty cost is calculated using V2G power as follows:

$$\begin{cases} \text{Cost}^{\text{U}}_{\text{EVl}} = \int_{P_{\text{EVshl}}}^{+\infty} \text{PF}^{\text{U}}_{\text{EVl}} \left(P_{\text{EVl}} - P_{\text{EVshl}}\right) \\ \quad \times f_{P_{\text{EV}}} \left(P_{\text{EVl}}\right) d P_{\text{EVl}} \\ = \frac{\text{PF}^{\text{U}}_{\text{EVl}}}{2} (m - P_{\text{EVshl}}) \times \\ \quad \left[1 + Gf\left(\frac{m - P_{\text{EVshl}}}{\sqrt{2}\sigma}\right) + \frac{\text{PF}^{\text{U}}_{\text{EVl}} . \sigma}{\sqrt{2\pi}} e^{-\frac{(m - P_{\text{EVshl}})^2}{2\sigma^2}}\right] \end{cases} \tag{23}$$

In the above equation $Gf\ (*)$ signifies the function of Gauss error; P_{EVl} and $\text{PF}^{\text{U}}_{\text{EVl}}$ are the output power and underestimated panalty factor of the lth EV unit.

2.4.2.3. EV overestimation cost When the available EV power is greater than the projected power, the overestimation cost becomes apparent. The overestimation costs of the lth EV unit are defined as follows.

$$\begin{cases} \text{Cost}^{\text{O}}_{\text{EVl}} = \int_{0}^{P_{\text{EVshl}}} \text{PF}^{\text{O}}_{\text{EVl}} \left(P_{\text{EVl}} - P_{\text{EVshl}}\right) . f_{P_{\text{EV}}} \left(P_{\text{EVl}}\right) d P_{\text{EVl}} \\ = \frac{\text{PF}^{\text{O}}_{\text{EVl}} \sigma}{\sqrt{2\pi}} \left(e^{-m^2/2\sigma^2} - e^{-(m - P_{\text{EVshl}})^2/2\sigma^2}\right) + \\ \frac{\text{PF}^{\text{O}}_{\text{EVl}}}{2} (m - P_{\text{EVshl}}) \times \left[Gf\left(\frac{m}{\sqrt{2}\sigma}\right) - Gf\left(\frac{m - P_{\text{EVshl}}}{\sqrt{2}\sigma}\right)\right] \end{cases} \tag{24}$$

where $\text{PF}^{\text{O}}_{\text{EVl}}$ is the overestimated panalty factor of the lth EV unit.

3 Problem formulation

The problem formulation of CHPED-based OPF in IEEE-57 bus system is an important optimization approach to supervision the power system operation. The problem formulation of the CHPED scheduling is to less utilization of thermal units for optimal power generation while satisfying the all constraints of generation and load balanced equation. The renewable energy sources also incorporated in the load balanced problem formulation of CHPED-based OPF system for economic power generation with less emission. The analytical form of cost equation, power balanced equation with and without renewable energy sources, equality and inequality constraints are illustrated as follows.

3.1 Objective function

3.1.1 Case 1: CHPED-based OPF system

The main purpose of proposed CHPED-based OPF system is represented by (25):

$$\begin{cases} \text{Minimum Cost} = \sum_{i=1}^{N_{\text{pou}}} \text{Cost}_{\text{poui}} \left(P_{\text{poui}}\right) \\ + \sum_{i=1}^{N_{\text{chp}}} \text{Cost}_{\text{chpi}} \left(P_{\text{chpi}}, H_{\text{chpi}}\right) + \sum_{i=1}^{N_{\text{hou}}} \text{Cost}_{\text{houi}} \left(H_{\text{houi}}\right) \end{cases} \tag{25}$$

where fuel cost of the power generator is manifested by $\text{Cost}_{\text{poui}} \left(P_{\text{poui}}\right)$; generation cost of co-generation and heat unit manifested with $\text{Cost}_{\text{ci}} \left(P_{\text{chpi}}, H_{\text{chpi}}\right)$ and $\text{Cost}_{\text{houi}} \left(H_{\text{houi}}\right)$; P_{poui} and H_{houi} signified the power and heat of ith unit; number of power, co-generation and heat only units manifested by N_{pou}, N_{chp}, N_{hou}.

The thermal cost function is described in the following equation and is expressed as a quadratic cost function.

$$\text{Cost}_{\text{poui}} \left(P_{\text{poui}}\right) = \alpha_{\text{poui}} \left(P_{\text{poui}}\right)^2 + \beta_{\text{poui}} P_{\text{poui}} + \gamma_{\text{poui}} \tag{26}$$

where α_{poui}, β_{poui} and γ_{poui} express the cost coefficients of the ith thermal unit.

By taking into account the valve point loading in in (27), the cost function equation examined in studied in (26) has been updated.

$$\begin{cases} C_{\text{poui}} \left(P_{\text{poui}}\right) = \alpha_{\text{poui}} \left(P_{\text{poui}}\right)^2 + \beta_{\text{poui}} P_{\text{poui}} + \gamma_{\text{poui}} \\ + \left|\delta_{\text{poui}} Sin\left\{\varepsilon_{\text{poui}} \times \left(P^{\min}_{\text{poui}} - P_{\text{poui}}\right)\right\}\right| \end{cases} \tag{27}$$

Due to sinusoidal terms from the quadratic equation and sinusoidal terms from the valve point loading, Eq. (27) becomes more nonlinear and non-differentiable. The valve point effects coefficients of the ith unit defined by δ_{poui} and $\varepsilon_{\text{poui}}$; the equation shown in (28) and (29) define the cost function of heat-only units and co-generation units.

$$\begin{cases} \text{Cost}_{\text{chpi}} \left(P_{\text{chpi}}, H_{\text{chpi}}\right) = \alpha_{\text{chpi}} \left(P_{\text{chpi}}\right)^2 + \beta_{\text{chpi}} P_{\text{chpi}} \\ + \gamma_{\text{chpi}} + \delta_{\text{chpi}} \left(H_{\text{chpi}}\right)^2 + \varepsilon_{\text{chpi}} H_{\text{chpi}} + \kappa_{\text{chpi}} H_{\text{chpi}} P_{\text{chpi}} \end{cases} \tag{28}$$

$$\text{Cost}_{\text{houi}} \left(H_{\text{houi}}\right) = \alpha_{\text{houi}} \left(H_{\text{houi}}\right)^2 + \beta_{\text{houi}} H_{\text{houi}} + \gamma_{\text{houi}} \tag{29}$$

In above expression, $\text{Cost}_{\text{chpi}} \left(P_{\text{chpi}}, H_{\text{chpi}}\right)$ and $\text{Cost}_{\text{houi}} \left(H_{\text{houi}}\right)$ define the cost equation of the ith co-generation unit and heat only unit, respectively.

3.1.2 Case 2: CHPED based OPF with wind–Solar

The cost function of wind-based CHPED problem is presented by (30).

$$\begin{cases} \text{Minimum Cost} = \sum_{i=1}^{N_{\text{pou}}} \text{Cost}_{\text{poui}}\left(P_{\text{poui}}\right) \\ \quad + \sum_{i=1}^{N_{\text{chp}}} \text{Cost}_{\text{chpi}}\left(P_{\text{chpi}}, H_{\text{chpi}}\right) \\ \quad + \sum_{i=1}^{N_{\text{hou}}} \text{Cost}_{\text{houi}}\left(H_{\text{houi}}\right) \\ \quad + \sum_{i=1}^{N_{\text{wind}}} \text{Cost}_{\text{windi}}\left(P_{\text{windi}}\right) + \sum_{i=1}^{N_{\text{solar}}} \text{Cost}_{\text{solari}}\left(P_{\text{solari}}\right) \end{cases} \tag{30}$$

In the above equation, $\text{Cost}_{\text{windi}}\left(P_{\text{windi}}\right)$ denotes the wind generation cost; number of wind units represented by N_{wind} respectively.

3.1.3 Case 3: CHPED-based OPF with wind–Solar–EV

The cost function of wind-based CHPED problem is presented by (31).

$$\begin{cases} \text{Minimum Cost} = \sum_{i=1}^{N_{\text{pou}}} \text{Cost}_{\text{poui}}\left(P_{\text{poui}}\right) \\ \quad + \sum_{i=1}^{N_{\text{chp}}} \text{Cost}_{\text{chpi}}\left(P_{\text{chpi}}, H_{\text{chpi}}\right) \\ \quad + \sum_{i=1}^{N_{\text{hou}}} \text{Cost}_{\text{houi}}\left(H_{\text{houi}}\right) + \sum_{i=1}^{N_{\text{wind}}} \text{Cost}_{\text{windi}}\left(P_{\text{windi}}\right) \\ \quad + \sum_{i=1}^{N_{\text{solar}}} \text{Cost}_{\text{solari}}\left(P_{\text{solari}}\right) + \sum_{i=1}^{N_{\text{EV}}} \text{Cost}_{\text{EVi}}\left(P_{\text{EVi}}\right) \end{cases} \tag{31}$$

In the above equation, $\text{Cost}_{\text{windi}}\left(P_{\text{windi}}\right)$ denotes the wind generation cost; number of wind units represented by N_{wind} respectively.

3.1.4 Emission minimization

The second single objective function's goal is to reduce emissions while ignoring cost minimization. Equation (32) is a mathematical depiction of thermal plant emission ($\text{emission}_{\text{pou}}$).

$$\text{Minimum emission}_{\text{pou}} = \sum_{t=1}^{T} \sum_{i=1}^{N_{\text{pou}}} \left[b_{i0} + b_{i1} P_{\text{poui}}^{t} + b_{i2} (P_{\text{poui}}^{t})^2 + b_{i3} \exp(b_{i4} P_{\text{poui}}^{t}) \right] \tag{32}$$

In (32), b_{i0}, b_{i1}, b_{i2}, b_{i3} and b_{i4} denote emission coefficients whereas $P_{\text{poui}}^{\text{t}}$ is the thermal power output.

3.1.5 Active power loss

Inherent resistance causes active power loss in transmission lines. Active power loss that has to be minimized is represented in (33):

$$P_{\text{L}} = \sum_{n=1}^{N_{\text{L}}} G_{n(pq)} \left(V_p^2 + V_q^2 - 2 V_p V_q \cos \varphi_{pq} \right) \tag{33}$$

$G_{n(pq)}$: transfer conductance of nth line connected between buses p and q. N_{L}: total number of transmission line. ϕ_{pq}: voltage angle between buses p and q.

3.1.6 Voltage deviation

To keep good voltage profile at load buses, voltage deviation at load buses has to be minimized and it is given by (34) :

$$\text{VD} = \sum_{l=1}^{N_B} |V_l - 1| \tag{34}$$

3.1.7 L-index

Under normal operating circumstances, it is crucial to maintain a consistent, appropriate bus voltage at each bus. The voltage stability indicator L-index is minimized in this work in order to improve voltage stability. The indicator values range from 0 to 1, with variations. Below, a quick discussion of a power system's L-index is provided. The relationship between the load and generator buses' voltage and current for a multi-node system can be described as follows (35) :

$$\begin{bmatrix} I_{l'} \\ I_{g'} \end{bmatrix} = \begin{bmatrix} y_{l'l'} & y_{l'g'} \\ y_{g'l'} & y_{g'g'} \end{bmatrix} \begin{bmatrix} V_{l'} \\ V_{g'} \end{bmatrix} \tag{35}$$

By matrix inversion, the above equation may be rearranged as follows (36):

$$\begin{bmatrix} V_{l'} \\ I_{g'} \end{bmatrix} = \begin{bmatrix} Z_{l'l'} & F_{l'g'} \\ K_{g'l'} & Y_{g'g'} \end{bmatrix} \begin{bmatrix} I_{l'} \\ V_{g'} \end{bmatrix} \tag{36}$$

The sub-matrix $F_{l'g'}$ may be expressed as under (37):

$$F_{l'g'} = -[y_{11}]^{-1} \left[y_{l'g'} \right] \tag{37}$$

The voltage stability index of the Kth bus may be expressed by (38).

$$L_k = |1 - \sum_{j=1}^{\text{Ng}} F_{kj} \frac{V_j}{V_k}| k = 1, 2, \ldots\ldots, N_l \tag{38}$$

3.1.8 Multi-objective function

Formerly single-objective functions are individually minimized. However in order to assess the effectiveness of the suggested method in a multi-objective context, two multi-objective functions are considered in this simulation study. Initially, employing penalty factor of ϵ_1, two single objective functions namely, cost and emission are transformed into a single fitness functions and it is illustrated as under (39):

$$F_1 = \text{Minimum}\,(\text{Cost} + \epsilon_1 \times \text{Emission}) \tag{39}$$

Here, in this simulation study, ϵ_1 is taken as 1200.

Furthermore, another multi-objective function is created to optimize the generation cost and L-index (i.e. L_k simultaneously with the proper penalty factor ϵ_2. The aforesaid multi-objective fitness function may be described as below 40:

$$F_2 = \text{Minimum}\,(\text{Cost} + \epsilon_2 \times L_k) \tag{40}$$

where ϵ_2 is taken as 100,000 in the present simulation study.

3.2 Constraints

3.2.1 Equality constraints

The constraints of CHPED-based OPF and CHPED-based OPF with wind are illustrated as given below.

3.2.1.1. Constraints of power balance for CHPED-based OPF Constraints of power balance for CHPED-based OPF system are given by:

$$\sum_{i=1}^{N_{\text{pou}}} P_{\text{poui}} + \sum_{i=1}^{N_{\text{chp}}} P_{\text{chpi}} = P_{\text{D}} + P_{\text{L}} \tag{41}$$

$$P_{\text{L}} = \sum_{i=1}^{N_{\text{pou}}}\sum_{j=1}^{N_{\text{pou}}} P_{\text{poui}} B_{ij} P_{\text{pouj}} + \sum_{i=1}^{N_{\text{pou}}}\sum_{j=1}^{N_{\text{chp}}} P_{\text{poui}} B_{ij} P_{\text{chpj}} + \sum_{i=1}^{N_{\text{chp}}}\sum_{j=1}^{N_{\text{chp}}} P_{\text{chpi}} B_{ij} P_{\text{chpj}} \tag{42}$$

$$\sum_{i=1}^{N_{\text{chp}}} H_i + \sum_{i=1}^{N_h} H_{\text{chpi}} = H_D \tag{43}$$

Equation (41) representation of power balance; transmission losses shown in Eq. (42); Eq. (43) represents heat balance. Thermal demand defined by H_{D} and B_{im}, B_{ij}, B_{jr} are power loss coefficients.

3.2.1.2. Power balance constraints for CHPED-based OPF with wind

CHPED-based OPF with wind power balance equation is defined by (44):

$$\sum_{i=1}^{N_{\text{pou}}} P_{\text{poui}} + \sum_{i=1}^{N_{\text{chp}}} P_{\text{chpi}} + \sum_{i=1}^{N_{\text{wind}}} P_{\text{windi}} = P_{\text{D}} + P_{\text{L}} \tag{44}$$

The power balance Eq. (41) is extended to a new solution as represented in (44), where wind power is incorporated with CHPED.

Power flow equation is shown in Eq. (45):

$$\begin{cases} \sum_{c=1}^{N_{\text{s}}} (P_{\text{Gc}} - P_{Lc}) = \sum_{c=1}^{N_{\text{s}}}\sum_{d=1}^{N_{\text{s}}} |V_c|\,|V_d|\,|Y_{cd}| \cos(\varphi_{cd} - \beta_{cd}) \\ \sum_{c=1}^{N_{\text{s}}} (Q_{\text{Gc}} - Q_{Lc}) = -\sum_{c=1}^{N_{\text{s}}}\sum_{d=1}^{N_{\text{s}}} |V_c|\,|V_d|\,|Y_{cd}| \sin(\varphi_{cd} - \beta_{cd}) \end{cases} \tag{45}$$

where P_{Lc} and Q_{Lc} is the active & reactive power demand of the cth bus; P_{Gc} and Q_{Gc} are the active and reactive power of generation and demand, respectively, of the cth bus; Y_{cd} is the admittance of transmission line connected between the cth and the dth bus; φ_{cd} is the admittance angle of transmission line connected between the cth and the dth bus; N_{s} is the number of buses.

3.2.2 Constraint of inequality

3.2.2.1. Constraints of capacity For steady operation, the limiting range of heat and power for power alone units, co-generation units, and heat only units is presented in (46)–(52). The voltage of power and co-generation units are displayed in (53)–(54). The constraints of load bus, transmission line and transformer tap changers are illustrated in (55)–(57). :

$$P_{\text{poui}}^{\min} \le P_{\text{poui}} \le P_{\text{poui}}^{\max} \quad \text{where}, i = 1, 2, 3, \ldots, N_{\text{pou}} \tag{46}$$

$$P_{\text{chpi}}^{\min}(H_{\text{chpi}}) \le P_{\text{chpi}} \le P_{\text{chpi}}^{\max}(H_{\text{chpi}}) \quad \text{where}, i = 1, 2, 3, \ldots, N_{\text{chp}} \tag{47}$$

$$P_{\text{windi}}^{\min} \le P_{\text{windi}} \le P_{\text{windi}}^{\max} \quad \text{where}, i = 1, 2, 3, \ldots, N_{\text{wind}} \tag{48}$$

$$P_{\text{Solari}}^{\min} \le P_{\text{Solari}} \le P_{\text{Solari}}^{\max} \quad \text{where}, i = 1, 2, 3, \ldots, N_{\text{Solar}} \tag{49}$$

$$P_{\text{EVi}}^{\min} \le P_{\text{EVi}} \le P_{\text{EVi}}^{\max} \quad \text{where}, i = 1, 2, 3, \ldots, N_{\text{EV}} \tag{50}$$

$$H_{\text{chpi}}^{\min}(P_{\text{chpi}}) \le H_{\text{chpi}} \le H_{\text{ci}}^{\max}(P_{\text{chpi}}) \quad \text{where}, i = 1, 2, 3, \ldots, N_{\text{chp}} \tag{51}$$

$$H_{\text{houi}}^{\min} \le H_{\text{houi}} \le H_{\text{houi}}^{\max} \quad \text{where}, i = 1, 2, 3, \ldots, N_{\text{hou}} \tag{52}$$

$$V_{\text{poui}}^{\min} \le V_{\text{poui}} \le V_{\text{poui}}^{\max} \quad \text{where}, i = 1, 2, 3, \ldots, N_{\text{pou}} \tag{53}$$

$$V_{\text{chpi}}^{\min} \le V_{\text{chpi}} \le V_{\text{chpi}}^{\max} \quad \text{where}, i = 1, 2, 3, \ldots, N_{\text{chp}} \tag{54}$$

(ii) Load bus constraints:

$$V_{\text{Lb}}^{\min} \le V_{\text{Lb}} \le V_{\text{Lb}}^{\max} \; b \in N_{\text{BL}} \tag{55}$$

(iii) Transmission line constraints:

$$S_{\text{Lb}} \le S_{\text{Lb}}^{\max} \; b \in N_{\text{LT}} \tag{56}$$

(iv) Transformer tap constraints:

$$T_{\mathrm{b}}^{\min} \le T_{\mathrm{b}} \le T_{\mathrm{b}}^{\max} \; b \in N_{\mathrm{T}} \tag{57}$$

There are shown the minimum and maximum power limits for ith power alone units and ith co-generation units are $P_{\mathrm{poui}}^{\min}$, $P_{\mathrm{poui}}^{\max}$, $P_{\mathrm{chpi}}^{\min}\left(H_{\mathrm{chpi}}\right)$ and $P_{\mathrm{chpi}}^{\max}\left(H_{\mathrm{chpi}}\right)$; $P_{\mathrm{windi}}^{\min}$ is the minimum power production of ith wind $P_{\mathrm{windi}}^{\max}$ is shown maximum power production of ith wind, $H_{\mathrm{chpi}}^{\min}$ and $H_{\mathrm{houi}}^{\min}$ are the minimum heat limit of the ith co-generation and heat unit; $H_{\mathrm{chpi}}^{\max}$ and $H_{\mathrm{houi}}^{\max}$ are depicted the maximum heat limit of the ith co-generation heat unit.

where $V_{\mathrm{Gb}}^{\min}$, $V_{\mathrm{Gb}}^{\max}$indicate respectively lower and upper voltage limits, for the bth generator bus; $P_{\mathrm{Gb}}^{\min}$, $P_{\mathrm{Gb}}^{\max}$ are the lower and upper bounds of active power generation, respectively, of the bth bus; $Q_{\mathrm{Gb}}^{\min}$, $Q_{\mathrm{Gb}}^{\max}$ are respective minimum and maximum reactive power generation margins of the bth bus; $V_{\mathrm{Lb}}^{\min}$, $V_{\mathrm{Lb}}^{\max}$ are the smallest and highest voltage edges, respectively, of the bth load bus, ${S_{\mathrm{Lb}}}^{\min}$, $S_{\mathrm{Lb}}^{\max}$ are the least apparent power flow and extreme apparent power flow limit, respectively, of the bth branch; $T_{\mathrm{b}}^{\min}$, $T_{\mathrm{b}}^{\max}$ are the bottom and extreme tap setting limits, respectively, of the bth regulating transformer; respectively.

4 Algorithm for optimization

4.1 DTBO

DTBO is introduced by Dehghani et al. [32]. The way driving instructor trains learners in a driving school, the scheme of DTBO mimics it. There are three phases in the mathematical structure of DTBO: (1) training by the driving instructor, (2) patterning of students from instructor skills, and (3) practice. In the process of driving training, intelligence of beginner is involved for being trained and acquiring the skill of driving. In the driving school, a learner driver can take lesson from numerous instructors. A learner develops its driving skill by following instructor's guidance and by its own practice. These interactions between learner and instructor and self-practice for developing driving skill are the fundamental base of Mathematical modeling of DTBO. DTBO is a metaheuristic method based on population. The DTBO population matrix (58) where each row member represents one of the solutions of the given problem is represented as follows:

$$Z = \begin{bmatrix} Z_1 \\ . \\ . \\ Z_p \\ . \\ . \\ Z_N \end{bmatrix}_{N\times m} = \begin{bmatrix} z_{11} & . & . & z_{1q} & . & z_{1m} \\ . & . & . & . & . & . \\ . & . & . & . & . & . \\ z_{p1} & . & . & z_{pq} & . & z_{pm} \\ . & . & . & . & . & . \\ . & . & . & . & . & . \\ z_{N1.} & . & . & z_{Nq} & . & z_{Nm} \end{bmatrix}_{N\times m} \tag{58}$$

Z is the DTBO population,Z_p. is the pth member of the population i.e. pth candidate solution of the problem, z_{pq} is the qth variable of the pth solution of the problem, N is population size, m denotes no of problem variables. At the beginning of DTBO implementation, the starting position of DTBO members (i.e. candidate solutions) is initialized randomly as given below (59):

$$\begin{aligned} & z_{pq} = z_{pq}^{\min} \\ & +r * \left(z_{pq}^{\max} - z_{pq}^{\min}\right) \quad for\ p = 1\ to\ N\ \varsigma\ q = 1\ to\ m \end{aligned} \tag{59}$$

where $z_{pq}^{\max}$, $z_{pq}^{\min}$ are the upper and lower limit, respectively, of the qth variable of the considered problem; r is a unbiased random value within 0 and 1. For every individual candidate solution, the value of the objective function is computed and it is represented as follows (60):

$$F = \begin{bmatrix} F_1 \\ . \\ . \\ F_p \\ . \\ . \\ F_N \end{bmatrix}_{N\times 1} = \begin{bmatrix} F\left(Z_1\right) \\ \\ \\ F\left(Z_p\right) \\ \\ \\ F\left(Z_N\right) \end{bmatrix}_{N\times 1} \tag{60}$$

The computed values of the objective function become the key criteria to judge the quality of the considered solutions. The candidate solution that produces best objective function value is taken as best member. With the iteration progress, best member is updated. The process of updating of candidate solution in DTBO follows three steps as follows:

Step 1 Training by the driving instructor (Exploration) From the population of DTBO, few best members are taken as driving instructors while the other members are considered as learner drivers. Selection of instructors and acquiring the instructor's skill provides the ability of global search to achieve optimal area for DTBO. In each iteration, comparing the values of objective function, L number (62) of DTBO members is chosen as instructors which are expressed as driving matrix DI (61)as follows:

$$DI = \begin{bmatrix} \{ DI_1 \\ . \\ . \\ DI_p \\ \\ DI_L \end{bmatrix}_{L\times m} = \begin{bmatrix} \{ DI_{11} \; . \; . \; DI_{1q} \; . \; DI_{1m} \\ . \; . \; . \; . \; . \\ . \; . \; . \; . \; . \\ DI_{p1} \; . \; . \; DI_{pq} \; . \; DI_{pm} \\ . \; . \; . \; . \; . \\ . \; . \; . \; . \; . \\ DI_{L1.} \; . \; . \; DI_{Lq} \; . \; DI_{Lm} \end{bmatrix}_{L\times m} \quad (61)$$

DI_p is pth driving instructor. DI_{pq} is qth variable of pth instructor.

$$L = \left\lfloor 0.1 \times N \times \left(\frac{1-s}{S}\right) \right\rfloor \quad (62)$$

s denotes current iteration and S is maximum iteration. In this step, the modified position of DTBO population member is obtained as given below (63):

$$z_{pq}^{\text{st1}} = \begin{cases} z_{pq} + r.\left(DI_{kpq} - I.z_{pq}\right), & F_{DIk_p} < F_p \\ z_{pq} + r.\left(z_{pq} - DI_{kpq}\right), & \text{otherwise} \end{cases} \quad (63)$$

Using Eq. (64), previous position is replaced by new position while it improves the objective function value.

$$Z_p = \begin{cases} Z_p^{\text{st1}}, & F_p^{\text{st1}} < F_p \\ Z_p, & \text{otherwise} \end{cases} \quad (64)$$

Z_p^{st1} is newly computed pth candidate solution at step 1 of DTBO, z_{pq}^{st1} is its qth problem variable, F_p^{st1} is its objective function value, I is a random number in the set 1,2, r is random value within 0 and 1. In DI_{kpq}, k is randomly selected from the set 1, 2, ...L i.e. kth driving instructor and $F_{DI}k_p$ is its objective function value, p indicates pth member of the population which is being trained by kth instructor.

Step 2 Patterning of the instructor skills of the student driver (Exploration) In the second step, instructor's skills and activities are imitated by learner driver for the improvement of solution in DTBO. Through this process DTBO members travel to different region of the search space. It enhances the power of DTBO's exploration. Through a linear combination among the DTBO members and instructors a modified position is created which is mathematically represented by Eq. (65). Using Eq. (66), the new position replaces the preceding position if the value of the objective function is improved than former.

$$z_{pq}^{\text{st2}} = \xi.z_{pq} + (1-\xi).DI_{kpq} \quad (65)$$

$$Z_p = \begin{cases} Z_p^{\text{st2}}, & F_p^{\text{st2}} < F_p \\ Z_p, & \text{otherwise} \end{cases} \quad (66)$$

Z_p^{st2} is the modified pth candidate solution on second stage of DTBO, z_{pq}^{st2} is its qth variable, F_p^{st2} is corresponding value of objective function. ξ is called patterning index described by Eq. (67):

$$\xi = 0.01 + 0.9\left(1 - \frac{s}{S}\right) \quad (67)$$

Step 3 Personal practice (Exploitation) In this step, the driving skills of the learner drivers are upgraded on the basis of personal practice. It is similar to exploit the power of local search of DTBO. Every learner tries to discover a better position in the vicinity of current position. New positions are created close to the current position by Eq. (68). If the new position improves objective function value than earlier then it replaces the earlier by Eq. (69).

$$z_{p.q}^{\text{st3}} = z_{pq} + (1-2r).R.\left(1 - \frac{s}{S}\right).z_{pq} \quad (68)$$

$$Z_p = \begin{cases} Z_p^{\text{st3}}, & F_p^{\text{st3}} < F_p \\ Z_p, & \text{otherwise} \end{cases} \quad (69)$$

Z_p^{st3} is the updated pth candidate solution at third step of DTBO, $z_{p,q}^{\text{st3}}$ is its qth variable, corresponding objective function value is F_p^{st3}, r is a random value between 0 and 1, R is 0.05, s is current iteration and S is the maximum iteration.

Through step 1 to step 3 population members of DTBO is updated which completes one DTBO iteration. After that next iteration starts with new updated population and this process continues [through Eqs. (61) to (69)] till final iteration is completed. At the end of final iteration best candidate solution is recorded as the solution of the problem.

4.2 Chaotic-based learning (CBL)

The majority of evolutionary algorithms take their cue from the population's constant search for the ideal solution and its random initialization. However, DTBO is still unable

to outperform other methods in locating the global optimal solution, which also influences the rate of convergence. The CDTBO is created by fusing chaos behavior with the DTBO in order to lessen this effect. The unpredictable and non-repeating properties of chaos allow for faster overall searches, which can be crucial for accelerating a metaheuristic algorithm's convergence.

To control the parameters of DTBO, different chaotic maps are integrated with DTBO in CDTBO technique. The chaotic set combination of ten chaotic maps with different behavior. For optimal solution the initial value taken as 0.7 within the range of 0 to 1. The various chaotic maps has been discussed in Table 2. The local optimal problem has been eliminated and provides global optimal solution using these chaotic maps.

4.3 Opposite number

The opposite number (70) is used in the candidate solution's mirror position. For a one-dimensional search space, the corresponding opposite number X_o of a randomly generated candidate solution X with interval [a, b] is denoted as follows:

$$X_o = a + b - X \tag{70}$$

where the search space's minimum and maximum limits are a and b, respectively. The preceding statement is stated similarly for n-dimensional search space by the following Eq. (71):

$$X_{ok} = a_k + b_k - X_k \tag{71}$$

where $k = 1, 2, ..., n$ and $X_k = X_1, X_2, ..., X_n$

4.4 Jumping rate

A new solution that outperforms the existing one in terms of fitness value is provided by jumping rate (72). The quasi-opposite solution is established following the development of new solutions using the jumping rate equation. The algorithm is assisted in finding the globally best solution by the choice of the jumping rate, which is between [0, 0.6].

$$j_{\mathrm{R}} = (j_{\mathrm{vR,Max}} - j_{\mathrm{R,Min}}) - (j_{\mathrm{R,Max}} - j_{\mathrm{R,Min}}) \left(\frac{f_{\mathrm{Max}} - f}{f_{\mathrm{Max}}} \right) \tag{72}$$

where j_{R} is jumping rate; $j_{\mathrm{R,Max}}$ denotes maximum jumping rate; minimum jumping rate is denoted by $j_{\mathrm{R,Min}}$; f is function for current iteration and f_{Max} is maximum number of iteration.

4.5 Use CODTBO in obtaining CHPED-based OPF solution

As it is mentioned that DTBO is integrated with CBL and OBL (known as CODTBO) in this work to enhance the efficiency of the technique, the flow chart of CODTBO is given in Fig. 4 and the steps of CODTBO algorithm applied on OPF are explained below :

Step 1 Randomly generate initial population Z which represents independent variables of the OPF problem such as all generator's active powers (excluding slack bus), voltages, and regulating transformers' tap settings. Z should not violate equality and inequality constraints.
Step 2 The chaotic map is used to initialize the random value. The chaotic number is updated using the chaotic map equation.
Step 3 Accomplish load flow by Newton–Raphson (NR) process [33] and evaluate entire dependent variables like slack bus active power, load voltages, etc from the Z and chaotic map.
Step 4 Compute the value of objective function for Z and chaotic map.
Step 5 Arrange the Z and chaotic map from best to worst according to value of the objective function.
Step 6 Choose N number of fittest members from Z and chaotic map to form new Z.
Step 7 Start DTBO
Step 8 Training by the driving instructor (Exploration)
Step 9 Comparing the value of objective function, obtain the driving instructor matrix DI.
Step 10 Chose a driving instructor in a random fashion from DI matrix.
Step 11 Using Eq. (63), find the new position for pth DTBO member.
Step 12 Verify if the constraints are within the limits or not by NR process
Step 13 Considering Eq. (64), the position of pth DTBO member is updated. The learner driver imitates the instructor's driving techniques (Exploration)
Step 14 Use Eq. (67) to compute the patterning index.
Step 15 Evaluate a new position for pth DTBO member by Eq. (65).
Step 16 Check if the constraints are within the limits or not by NR process
Step 17 Use Eq. (66), to update the position of pth DTBO member.
Step 18 Personal practice (Exploitation)
Step 19 Compute the new position of pth DTBO member by (68).
Step 20 Confirm if the constraints are within the limits or not by NR process

Table 2 List of various chaotic maps

Sl. no.	Name	Chaotic map
N1	Circle	$r_{k+1} = r_{k+b} - (a/2\pi)\sin(2\pi k) \bmod (2)$
N2	Cubic	$r_{j+1} = ar_j\left(1 - r_j{}^2\right)$
N3	Chebyshev map	$r_{j+1} = \cos\left(k\cos^{-1}(r_k)\right)$
N4	Logistic map	$r_{k+1} = ar_k(1 - r_k)$
N5	Gussian map	$r_{k+1} = r_{k+1}\left\{0,\ r_k = 0,\ \frac{1}{r_k} \bmod (1) = \frac{1}{r_k} - \left[\frac{1}{r_k}\right]\right.$
N6	Liebovitch map	$r_{k+1} = ar_k(1 - r_k)$
N7	Iterative map	$r_{k+1} = \mathrm{Sin}\left(\frac{a\pi}{rk}\right), a \in (\mathrm{U},1)$
N8	Sine	$X_{i+1} = a/4\left(\sin\prod x\right)$
N9	Sinusoidal	$X_{i+1} = a(X_i)\,2\left(\sin\prod x_i\right)$
N10	Tent	$X_{i+1} = \begin{cases} \frac{X_i}{0.7};\ \mathrm{X}_i < 0.7 \\ \frac{10}{3}(1 - X_i);\ \mathrm{X}_i \geq 0.7 \end{cases}$

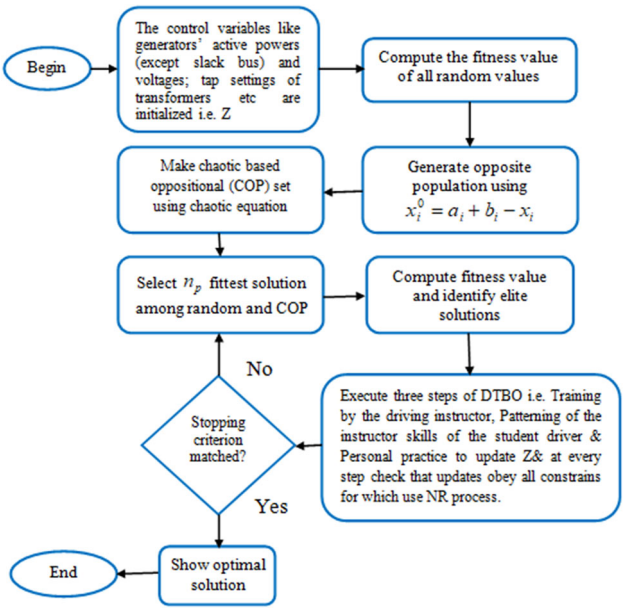

Fig. 4 Flowchart of CODTBO optimization technique

Step 21 Use Eq. (69), to update the position of pth DTBO member.

Step 22 End DTBO

Step 23 After generating new populations by DTBO, the COL is calculated and fitness value COL is calculated.

Step 24 Go to step 5 for next iteration till stopping criterion is reached

Step 25 Output: The best candidate solution achieved by CODTBO.

5 Simulation result

5.1 CEC benchmark system

A variety of benchmark functions are included in the IEEE CEC Benchmark System, which is intended to assess the behavior and performance of different multi-objective combinatorial optimization tasks (MCTs). The MCTs' capacity to investigate various solutions, intensify toward ideal solutions, and converge successfully is evaluated using these functions. There are various configuration options for the IEEE CEC Benchmark System, including 10D, 30D, 50D, and 100D dimensions. However, we specifically use 30D and 50D dimensions to analyze the IEEE CEC 2017 benchmark system in this study. Numerous functions that fall into the categories of unimodal, multi-modal, hybrid, and composite are present in the IEEE CEC 2017 benchmark system. These functions are taken from [34]. The ability of the optimization process to intensify toward a single optimal solution is evaluated using unimodal functions. Multi-modal functions assess how well the algorithm explores different solutions. Multimodal and unimodal features are united to make hybrid functions. Two or more unimodal & multimodal functions are merged to form composite functions. We set a maximum limit of function assessments at $10^4 \times D$ for every experiment function in both the IEEE CEC benchmark systems, and we fully appraise the algorithm's performance through 30 separate runs. As previously stated, the test functions of the benchmark system under examination might be divided in various groups: $F1 - F3$, $F4 - F16$, $F17 - F22$, and $F23 - F30$ are unimodal, multimodal, hybrid & composite functions, respectively. It is noteworthy to emphasize that F2 is excluded from the IEEE CEC 2017 benchmark system due to its unstable properties, as documented in [34]

Table 3 Statistical comparison of the proposed CODTBO with BWM_HS, CVnew, SGSADE, HGSO, LSHADE-cnEpSin and LSHADE-SPACMA on CEC 2017 with 30D considering $F1$–$F16$

CEC 2017 ($D = 30$)								
Function		BWM_HS	CVnew	SGSADE	HGSO	LSHADE -cnEpSin	LSHADE -SPACMA	CODTBO
Unimodal								
	Mean	3.824E+03	1.223E+10	3.559E−08	5.524E+03	0.000E+00	2.966E−08	3.524E−08
F1	SD	4.837E+03	0.000E+00	3.957E−08	1.123E+03	0.000E+00	2.054E−08	2.032E−08
	Sign	+	+	−	−	−	−	
	Mean	1.215E−07	1.523E+02	1.341E+02	5.962E+02	2.122E−08	3.306E−08	2.012E−07
F3	SD	4.523E−08	9.463E+01	1.182E+02	2.883E+02	2.225E−08	2.056E−08	2.112E−07
	Sign	+	+	+	+	+	+	
Multi-modal								
	Mean	6.821E+01	1.562E+01	1.423E+01	4.732E+02	4.355E+01	3.221E−08	2.792E−08
F4	SD	3.077E+01	2.855E+01	2.621E+01	3.024E+02	2.930E+00	2.432E−08	1.242E−08
	Sign	+	+	+	+	+	−	
	Mean	5.023E+01	1.325E+02	8.862E+01	6.223E+02	1.456E+01	3.721E+00	3.065E+01
F5	SD	1.892E+01	2.774E+01	1.806E+01	9.921E+00	2.442E+00	2.642E+00	1.011E+01
	Sign	+	+	+	+	−	−	
	Mean	1.224E−05	2.113E+01	2.252E−08	5.972E+02	1.098E−08	1.321E−08	8.142E+00
F6	SD	2.153E−05	8.112E+00	1.542E−08	7.662E+00	1.456E−08	1.332E−08	1.021E−07
	Sign	−	+	−	+	−	−	
	Mean	5.992E+01	2.326E+02	1.315E+02	8.421E+02	4.902E+01	3.551E+01	5.994E+00
F7	SD	9.663E+00	2.112E+01	1.654E+01	6.232E+01	2.221E+00	8.224E−01	5.378E−01
	Sign	+	+	+	+	+	+	
	Mean	4.994E+01	1.226E+02	8.321E+01	8.221E+02	1.301E+01	3.750E+00	3.291E+00
F8	SD	1.284E+01	2.697E+01	1.584E+01	2.583E+01	2.816E+00	1.758E+00	2.623E+00
	Sign	+	+	+	+	+	=	
	Mean	1.122E+01	2.201E+03	5.963E−08	1.758E+03	0.224E+00	0.361E+00	0.000E+00
F9	SD	8.0023E+01	8.473E+02	6.012E−08	2.383E+02	0.225E+00	0.685E+00	5.223E−08E+00
	Sign	+	+	+	+	+	+	
	Mean	2.723E+03	4.512E+03	5.124E+03	5.223E+03	1.098E+03	1.877E+03	4.002E+02
F10	SD	4.778E+02	3.023E+02	5.527E+02	3.122E+02	2.421E+02	3.555E+02	8.912E+01
	Sign	+	+	+	+	+	+	
	Mean	9.462E+01	3.674E+01	5.022E+01	1.433E+03	1.776E+01	4.202E+00	3.427E+00
F11	SD	3.223E+01	1.928E+01	3.112E+01	2.884E+01	2.012E+01	3.692E+00	1.815E+00
	Sign	+	+	+	+	+	=	
	Mean	5.023E+05	5.112E+09	1.893E+04	5.045E+04	4.227E+02	4.997E+02	4.993E+00
F12	SD	4.492E+05	5.928E+09	6.994E+03	3.112E+04	1.492E+02	2.793E+02	4.012E+00
	Sign	+	+	+	+	+	+	
	Mean	1.892E+04	7.995E+01	2.993E+02	5.436E+04	2.227E+01	0.988E+01	7.342E−01
F13	SD	2.202E+04	2.887E+01	3.042E+02	2.114E+03	0.998E+01	5.023E+00	4.068E−01
	Sign	+	+	+	+	+	+	
	Mean	4.023E+03	5.056E+01	6.141E+01	2.321E+03	1.998E+01	2.783E+01	3.112E−01
F14	SD	3.272E+03	7.118E+00	8.873E+00	1.768E+00	2.493E+00	2.112E+00	0.692E−01
	Sign	+	+	+	+	+	+	
	Mean	8.016E+03	3.815E+01	4.992E+01	3.774E+03	4.002E+00	4.653E+00	4.112E+01

Table 3 continued

CEC 2017 ($D = 30$)								
Function		BWM_HS	CVnew	SGSADE	HGSO	LSHADE -cnEpSin	LSHADE -SPACMA	CODTBO
F15	SD	8.886E+03	8.772E+00	3.012E+01	5.008E+02	2.055E+00	2.992E+00	1.334E+01
	Sign	+	=	+	+	−	−	
	Mean	4.992E+02	7.456E+02	5.066E+02	3.322E+03	2.692E+01	4.213E+01	5.882E+00
F16	SD	1.998E+02	2.023E+02	1.778E+02	3.402E+02	2.996E+01	5.774E+01	3.054E+00
	Sign	+	+	+	+	+	+	

5.1.1 CEC 2017 (30D)

In the perspective of 30 dimensions (30D), Table 3 displays statistical findings illustrating the best mean error values and standard deviations (SD) attained by the suggested CODTBO and other MCTs for together unimodal and multimodal benchmark functions. It is worth mentioning that for all participating MCTs, mean error values less than 10e-08 are regarded as 0. Table 3 reveals unequivocally that our suggested MCT beats most of the other state-of-the-art MCTs used in this work for the bulk of the test functions with respect to mean error values. This better performance in achieving optimal values for unimodal and multimodal test functions indicates that, in comparison to the other MCTs under consideration, the changes we have made to our suggested MCT have successfully improved its capacity for intensification and diversification. Additionally, it is clear from looking at the SD values in Table 3 that the suggested CODTBO has the best degree of precision out of all the MCTs that are taken into consideration. The comparison of the best mean error values and SD produced by various MCTs for hybrid and composite functions is shown in Table 4. In contrast to the other MCTs in the experiment, the results in Table 4 demonstrates that the suggested CODTBO performs better in terms of mean error values and SD, indicating its potential to produce extremely accurate and high-quality solutions. In order to examine the statistical significance, the mean error values of the suggested MCT and the other MCTs for each test function are compared using a Wilcoxon signed-rank test with a significance level of 0.05 [35]. Based on the signed-rank test findings, the competing MCTs are allocated "+", "=", and "−" signs according to how well they perform statistically against the proposed CODTBO. The "+", "=", and "−" indications denote whether the performance of an MCT is inferior to, equal to, or superior than the suggested CODTBO. This is an essential distinction to make. The statistical robustness of the proposed CODTBO over its competitors is confirmed by Table 4, which shows that the proposed MCT obtains the most "+" signs in comparison to other participating MCTs. To further evaluate the overall statistical performance of the suggested MCT, the Friedman rank test [35] is performed. The suggested CODTBO ranks first out of all the MCTs that are taken into consideration based on the Friedman rank.

5.1.2 CEC 2017 (50D)

The best mean error values and standard deviations (SD) attained by the suggested CODTBO and additional participating MCTs for the 50D case are shown in Table 4. The performance of the proposed CODTBO is clearly extremely competitive across most uni-modal and multi-modal functions, as can be seen from the best mean error values given in Table 4. Moreover, it is evident from looking at the SD values that the suggested technique regularly performs better than the other approaches that are being considered. When evaluating the best mean error values and SD for the majority of hybrid and composite functions, the suggested method performs better than other methods, as shown in Table 4. The Wilcoxon signed-rank test findings, which are displayed in Table 5, further support the statistical superiority of the suggested CODTBO since it obtains more "+" signs than the other qualified MCTs. Lastly, there is clear evidence from Table 5's bottom row that the suggested CODTBO ranks top among all participating MCTs based on the Friedman rank test.

5.2 Optimal power flow-based CHPED

For optimal power flow in the transmission line with the best possible objective function solution, CHPED is combined with the IEEE 57 bus system in the current study. Two test systems are used in the current simulation investigation for the CHPED–OPF problem of the power system. On these test systems, the CODTBO algorithm is used to demonstrate the usefulness and efficiency of CHPED. By comparing the results with tested DTBO, ODTBO on the suggested system, the superiority of the provided CODTBO algorithm has been demonstrated. Doing the simulation in MATLAB 2014 allows for testing. A newer core i5 CPU with internal memory rated at 2.5 GHz and 8 GB of RAM powers the PC used to run MATLAB. In this part, the suggested algorithm's simulation results and calculation times for test systems 1, 2

Table 4 Statistical comparison of the proposed CODTBO with BWM_HS, CVnew, SGSADE, HGSO, LSHADE-cnEpSin and LSHADE-SPACMA, on CEC 2017 with 30D considering $F17$–$F30$

CEC-2017 ($D = 30$)								
Function		BWM_HS	CVnew	SGSADE	HGSO	LSHADE -cnEpSin	LSHADE -SPACMA	CODTBO
Hybrid								
	Mean	3.123E+02	2.023E+02	8.114E+01	2.007E+03	3.232E+01	2.998E+01	1.972E+01
F17	SD	1.947E+02	6.887E+01	2.212E+01	1.997E+01	4.997E+00	7.338E+00	1.086E+01
	Sign	+	+	−	+	−	−	
	Mean	1.483E+05	4.012E+01	1.996E+03	0.997E+04	1.992E+01	3.765E+01	1.792E+03
F18	SD	5.886E+04	6.993E+00	1.786E+03	5.675E+04	6.872E−01	2.002E+00	1.777E−01
	Sign	+	−	=	+	−	−	
	Mean	7.884E+03	1.934E+01	2.227E+01	1.978E+03	4.453E+00	8.198E+00	7.552E−01
F19	SD	9.872E+03	3.096E+00	6.203E+00	2.893E+03	1.869E+00	2.242E+00	6.173E+00
	Sign	+	+	+	+	+	+	
	Mean	1.842E+02	1.756E+02	0.883E+02	1.675E+03	2.466E+01	7.756E+01	3.162E+02
F20	SD	8.889E+01	9.552E+01	4.888E+01	2.997E+02	6.432E+00	4.162E+01	2.025E+01
	Sign	+	+	+	+	=	+	
	Mean	2.586E+02	1.765E+02	2.776E+02	2.965E+03	1.912E+02	1.834E+02	6.122E+00
F21	SD	1.496E+01	2.678E+01	2.223E+01	2.512E+01	2.769E+00	3.432E+00	1.012E+00
	Sign	+	+	+	+	+	+	
	Mean	1.876E+03	1.234E+03	1.765E+02	3.971E+03	2.888E+02	2.592E+02	1.267E+01
F22	SD	1.621E+03	1.844E+03	1.223E+01	8.340E+02	1.503E+01	2.844E+01	8.342E+00
	Sign	+	+	=	+	=	=	
Composite								
	Mean	4.023E+02	3.786E+02	3.972E+02	1.882E+03	2.658E+02	2.142E+02	4.042E+01
F23	SD	4.987E+01	4.677E+00	2.719E+01	5.432E+01	2.993E+01	3.453E+01	1.129E+00
	Sign	+	+	+	+	+	+	
	Mean	5.023E+02	4.476E+02	3.123E+04	2.121E+03	4.112E+02	1.887E+01	2.425E+02
F24	SD	2.228E+01	2.564E+02	2.223E+01	8.645E+01	2.453E+00	1.675E+00	3.778E+01
	Sign	+	+	+	+	+	+	
	Mean	3.874E+02	3.586E+02	4.112E+02	2.978E+02	2.342E+02	1.987E+01	1.828E+01
F25	SD	2.387E+00	7.234E−01	4.889E+00	2.986E+01	7.334E−03	1.768E−02	1.556E−03
	Sign	+	+	+	+	+	+	
	Mean	2.675E+03	3.678E+02	2.876E+03	4.675E+03	9.251E+02	9.741E+02	1.127E+02
F26	SD	6.345E+02	3.123E+01	2.032E+02	1.987E+02	4.665E+01	3.570E+01	3.027E+01
	Sign	+	+	+	+	+	+	
	Mean	5.573E+02	5.256E+02	5.512E+02	3.654E+03	5.117E+02	5.231E+02	4.212E+02
F27	SD	1.382E+01	9.867E+00	1.786E+00	1.132E+02	6.568E+00	1.823E+01	1.675E+00
	Sign	=	=	=	+	=	=	
	Mean	4.455E+02	3.265E+02	3.564E+02	3.198E+03	2.864E+02	2.998E+02	8.675E+01
F28	SD	6.453E+01	3.876E+01	5.132E+01	7.475E+01	3.912E+01	5.785E+01	3.274E+01
	Sign	+	+	+	+	+	+	
	Mean	5.114E+02	8.342E+02	6.432E+02	3.786E+03	4.346E+02	3.894E+02	6.941E+02
F29	SD	1.765E+02	1.231E+02	6.543E+01	1.346E+02	7.128E+00	4.012E+01	1.234E+02
	Sign	+	+	+	+	+	+	
	Mean	1.022E+04	2.342E+03	2.643E+03	9.765E+03	1.475E+03	8.754E+02	8.224E+02
F30	SD	5.743E+03	5.123E+02	9.368E+02	3.542E+03	4.302E+03	9.123E+02	2.781E+02
	Sign	=	−	−	=	−	−	

Table 5 The results of the Wilcoxon signed-rank test and Friedman rank test, considering the mean error value for CEC 2017 ($D = 50$)

Sign	CODTLBO	Vs.	BWM_HS	CVnew	SGSADE	HGSO	LSHADE -cnEpSin	LSHADE -SPACMA
+/=/−			27/00/02	22/02/05	26/00/03	28/00/01	17/04/08	18/03/08
Statistical Rank		BWM_HS	CVnew	SGSADE	HGSO	LSHADE -cnEpSin	LSHADE -SPACMA	CODTBO
Friedman Rank		5.618	4.804	5.191	7.122	2.870	2.436	1.427
Overall Rank		6	4	5	7	3	2	1

Table 6 Cost and emission coefficients of thermal units for IEEE 57-bus system

Generator	Bus	a	b	c	d	e	α	β	γ	ω	μ
TG1 (POU)	1	0	2	0.00375	18	0.037	4.091	−5.554	6.49	0.0002	2.857
TG2 (POU)	2	0	1.75	0.0175	16	0.038	2.543	−6.047	5.638	0.0005	3.333
TG3 (CHP)	3	0	3	0.025	13.5	0.041	6.131	−5.555	5.151	0.00001	6.677
TG6 (CHP)	6	0	2	0.00375	18	0.037	3.491	−5.754	6.39	0.002	2.667
TG8 (CHP)	8	0	1	0.0625	14	0.04	4.258	−5.094	4.586	0.000001	8
TG9 (CHP)	9	0	1.75	0.0195	15	0.039	2.754	−5.847	5.238	0.0004	2.88
TG12 (CHP)	12	0	3.25	0.00834	12	0.045	5.326	−3.555	3.38	0.002	2.00

Table 7 Generation limits and cost co-efficient of HOU

UNIT	Bus	Hmin (MWTh)	Hmax (MWTh)	α	β	γ
HOU	31	0	2695.2	0.038	2.0109	950

and 3 are provided. Also, it is explained how realistic an feasible range the various co-generation units' power and heat production falls under. The current CODTBO algorithm achieves the greatest results in the shortest amount of time at population size 50. There are 100 iterations for each population for each case. Cost and emission coefficients of thermal units for IEEE 57-bus system are depicted in Table 6. Generation limits and cost co-efficient of HOU are displayed in Table 7. Wind and solar parameters are shown in Table 8. Moreover, CODTBO has been used in all three test systems once the renewable sources have been added. For test systems using renewable energy sources, the simulation outcomes of CODTBO, ODTBO and DTBO are contrasted. Table 9 lists the fifteen various situations over single and multi-objective functions of three systems that are examined in this paper. The simulation results indicate that using renewable sources lowers generation costs compared to OPF-CHPED systems based on non-renewable energy.

5.3 Test system 1

With IEEE-57 buses, test system 1 comprises of four power, two CHP, and one heat units. There are 80 branches that connect the 57 buses. Four power units are installed in buses 1, 2, 3, and 6 while two CHP units are associated to buses 9 and 12 and one heat only unit connect with bus 58. The total amount of load demand is 1250.8 MW whereas reactive power and heat demand are 336.4 MVar and 175 MWth. Seven scheduled active power, seven total generator bus voltages, fifteen tap-changing transformers, three compensation devices and three heat-only units are used as the control variables. For 24 buses, the load voltage is measured between 0.94 and 1.06 p.u. An overview of IEEE 57

Table 8 Wind speed and solar irradiance distribution parameters, rated power of wind and solar plants and associated cost coefficients

Wind power generators plants						Solar power system	
				Cost coefficient ($/MWh$)			
Wind farm	No. of. turbines	Rated power Pwr (MW)	Weibull PDF parameters	Reserve, KRw	Penalty, KPw	Rated power (MW)	lognormal parameters
WG5 (bus 5)	25	75	$\xi = 9,\ \kappa = 2$	3	1.5	0.96	0.96
WG11 (bus 11)	20	60	$\xi = 10, \kappa = 2$	3	1.5	0.96 50 (bus 13)	0.96 $\varepsilon = 6, \lambda = 0.6$

Table 9 Various case-studies investigated in this article

Case	Single objective	Multi-objective	Considered objectives	Constraints	Test system
1	✓		Total Cost minimization with valve point effects	Equality and non-equality	
2	✓		Emission minimization	Equality and non-equality	
3		✓	Simultaneous minimization of Cost and Emission	Equality and non-equality	
4	✓		Voltage stability minimization	Equality and non-equality	
5		✓	Simultaneous minimization of Cost with voltage stability	Equality and non-equality	IEEE 57 Bus
6	✓		Total Cost minimization with valve point effects for thermal, wind and solar energy	Equality and non-equality	
7	✓		Emission minimization	Equality and non-equality	
8		✓	Simultaneous minimization of Cost with Emission	Equality and non-equality	
9	✓		Voltage stability minimization	Equality and non-equality	
10		✓	Simultaneous minimization of Cost with voltage stability	Equality and non-equality	Wind–solar based IEEE 57 Bus
11	✓		Total Cost minimization with valve point effects for thermal, wind, solar and EV	Equality and non-equality	
12	✓		Emission minimization	Equality and non-equality	
13		✓	Simultaneous minimization of Cost with Emission	Equality and non-equality	
14	✓		Voltage stability minimization	Equality and non-equality	
15		✓	Simultaneous minimization of Cost with voltage stability	Equality and non-equality	Wind–solar–EV based IEEE 57 Bus

Table 10 An overview of IEEE 57 bus for OPF-based CHPED system

Items	Quantity	Details
Buses	57	[ref]
Branches	80	[ref]
Thermal generators	7	5 power only units (buses 1,2,3,6 and 8), 2 CHP units (buses 9 and 12) and 1 heats only unit (bus 58)
Tap changing transformer	15	Branches:19, 20, 31, 37, 41, 46, 54, 58, 59, 65, 66, 71, 73, 76 and 80
		Scheduled real power for 6 Nos. Generators; bus voltages of all generator buses (7 Nos.)
Control variables	34	Transformer tap setting (15 nos), compensation devices (3 Nos.), 3 heat units.
Load demand, Heat demand		1250.8 MW, 336.4 MVAr, 175 MWth
Range of load bus voltage	24	[0.94-1.06] p.u.
Compensation devices	2	Buses: 18, 25 and 53

bus for OPF-based CHPED system has been displayed in Table 10. Co-generation units' capacity to produce both heat and power located in feasible operating region displayed in Fig. 5. The proposed test system 1 has discussed a total of five scenarios for single- and multi-objective functions. The single-objective functions include minimizing total cost, emissions and stability -index. The multi-objective functions include minimizing cost with emission and cost with voltage stability simultaneously. Using DTBO the obtained optimal cost is 31,876.80 ($/h), emission 1.7641 (t/h) and L-index is 0.2443, whereas for multi-objective function simultaneously minimized total cost and emission are 32,919.8 ($/h) and 2.5318 (t/h). Again simultaneously minimized total cost with voltage stability are 33,828.42 ($/h) and 0.2605. After

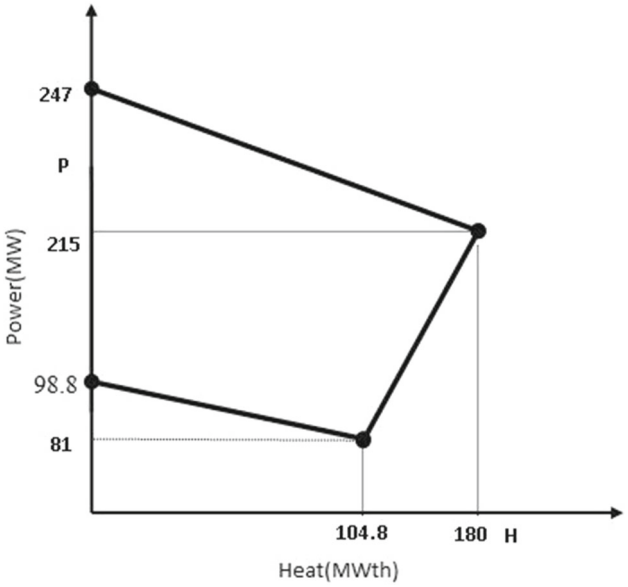

Fig. 5 Feasible region of CHP units

that CODTBO method has been tested the obtained optimal cost is 30,863.9779 ($/h), emission 1.7585 (t/h) and L-index is 0.2391 whereas for multi-objective function simultaneously minimized total cost and emission are 31161.2468 ($/h) and 2.5114 (t/h). Again simultaneously minimized total cost with voltage stability are 32,347.5352 ($/h) and 0.2584. The results has been displayed in Table 11 which justified the effectiveness of CODTBO over ODTBO and DTBO to obtained the optimal solution in all respect. The variation of control variables for five cases has been illustrated in Fig. 6. Five cases of the OPF with CHPED system were evaluated with DTBO, ODTBO and CODTBO, and comparisons were done to judge the superiority of the CODTBO technique. The different comparison of CHPED-based OPF system on cost and stability index are displayed in Figs. 7 and 8. The convergence graph of the presented CODTBO, ODTBO and DTBO optimization techniques illustrated in Fig. 9 The optimal solution using CODTBO of different objectives has been reached within less iterations rather than DTBO. This comparison studies established the fastness of computational time of CODTBO for integrating the chaotic-based learning with DTBO optimization technique. The comparison of statistical analysis after 100 iterations with minimum value, maximum value and average value of proposed DTBO, ODTBO and CODTBO has been displayed in Table 15. The difference of minimum value, maximum value and average value is much closer using CODTBO respect to DTBO which is the evidence of robustness of suggested CODTBO technique.

5.3.1 Test system-2

Furthermore to get the effective solution over cost minimization and emission minimization with optimal power flow in transmission line renewable sources like wind and solar energy are integrated with proposed CHPED-based OPF system. The system became more complex due to presence of uncertainties of wind speed. In CHPED system four-power only units, two co-generation units and one heat only unit are integrated. In this proposed wind and solar-based CHPED–OPF system one power only unit is replaced with wind unit and another power only unit replaced with solar unit. In IEEE-57 bus system bus-2 and bus-3 are connected with wind and solar generating unit. The total amount of load demand is 1250.8 MW, whereas reactive power and heat demand are 336.4 MVar and 175 MWth. An overview of IEEE 57 bus system for wind, solar-based OPF-CHPED is depicted in Table 12. The simulation results of DTBO and CODTBO and optimal setting of control variables are illustrated in Table 13. The DTBO, ODTBO and CODTBO has been applied on the proposed renewable-based CHPED–OPF system and analogy study to judge the excellency of the proposed optimization method on single-objective and multi-objective functions. Using DTBO the obtained optimal cost is 30,237.2572 $/h, emission 1.6822 (t/h) and L-index is 0.2379, whereas for multi-objective function simultaneously minimized cost and emission are 30589.546 $/h and 2.5145 (t/h) again simultaneously minimized cost with stability index are 32018.1764 and 0.2571. After the CODTBO method has been tested, the obtained optimal cost is 30,057.0093 $/h, emission 1.6598 (t/h), and reduced L-index is 0.2362, whereas for multi-objective function simultaneously minimized cost and emission are 30,337.5731 $/h and 2.4672 (t/h). After that simultaneously minimized cost with stability index are 31,654.4568 $/h and 0.2521. The statistical analysis has been done using DTBO, ODTBO and CODTBO on a renewable-based OPF-CHPED system and displayed in Table 15 which is the evidence of the robustness of the proposed CODTBO technique. The comparison of DTBO, ODTBO, CODTBO on emission of wind–solar CHPED-based OPF system is displayed in Fig. 10. The convergence characteristics of different objective functions are shown in Fig. 11, when the CODTBO optimisation technique yields results that converge to the optimum value in every situation much earlier than the DTBO and ODTBO techniques. From simulation result it has been observed that after incorporating renewable energy sources with CHPED-based OPF system CODTBO method provided optimal solution than other tested techniques, it also proved that proposed CODTBO has better dealing capability with nonlinear functions.

Table 11 Simulation results and control parameters of different cases for CHPED-based OPF system of IEEE-57 bus

Control parameters	Min.	Max.	CASE 1 [CODTBO]	CASE 1 [DTBO]	CASE 2 [CODTBO]	CASE 2 [DTBO]	CASE 3 [CODTBO]	CASE 3 [DTBO]	CASE 4 [CODTBO]	CASE 4 [DTBO]	CASE 5 [CODTBO]	CASE 5 [DTBO]
PTG1 (MW)	0	575.88	567.82	569.9	346.37	346.92	553.17	554.51	528.83	548.24	575.29	569.84
PTG2 (MW)	30	100	99.75	97.51	98.79	99.87	99.02	98.58	30.05	34.53	99.93	95.07
PTG3 (MW)	40	140	138.4	112.38	138.38	138.54	137.87	132.35	96.19	51.59	138.74	133.07
PTG6 (MW)	30	100	95.67	97.51	98.46	98.83	92.1	88.28	94.65	92.02	96.16	96.09
PTG8 (MW)	100	550	406.41	429.58	464.86	465.71	396.43	399.27	461.23	492.23	409.22	377.12
PTG9 (MW)	30	100	95.33	93.69	99.66	99.67	93.45	94.61	97.05	99.98	97.05	96.32
PTG12 (MW)	100	410	107.98	109.73	240.91	240.31	135.17	150.11	241.21	232.12	128.1	176.57
V1 (p.u.)	0.94	1.06	0.9718	0.9659	0.9455	0.9428	0.9574	0.9779	1.0579	1.0505	1.0577	1.0581
V2 (p.u.)	0.94	1.06	0.9578	0.9578	0.9647	0.9587	0.948	0.9787	0.9458	0.9417	1.0544	1.0526
V3 (p.u.)	0.94	1.06	0.9533	0.9436	0.9444	0.9523	0.9491	0.945	1.0481	1.0504	1.0521	1.0296
V6 (p.u.)	0.94	1.06	0.9487	0.9428	0.9557	0.9893	0.945	0.9635	1.06	1.0533	1.0388	1.0535
V8 (p.u.)	0.94	1.06	0.9572	0.941	0.955	0.9643	0.9505	0.9445	1.0571	1.0546	1.0597	1.0586
V9 (p.u.)	0.94	1.06	0.9409	0.9439	0.9483	0.942	0.9422	1.0119	1.0566	1.0563	1.0321	1.054
V12 (p.u.)	0.94	1.06	0.9424	0.9411	0.9414	0.9464	0.9464	0.9497	1.0587	1.0575	1.0344	1.0453
T19 (4–18) (p.u.)	0.9	1.1	0.9921	0.9542	0.9009	0.9115	0.977	1.0796	0.9002	0.9273	0.9168	0.9971
T20 (4–18) (p.u.)	0.9	1.1	0.9636	0.9067	1.0516	0.9155	0.9795	1.0166	0.9339	0.9119	0.923	0.982
T31 (21–20) (p.u.)	0.9	1.1	1.0087	0.9274	1.0271	0.9597	1.0557	1.0754	1.0806	1.0852	1.0417	1.0589
T37 (24–26) (p.u.)	0.9	1.1	0.9527	1.048	0.9373	1.0147	1.0015	0.9547	1.0944	1.089	1.0843	1.098
T41 (7–29) (p.u.)	0.9	1.1	0.9082	1.0432	0.9285	0.9372	0.9152	0.9113	0.9121	0.9142	0.9118	0.9063
T46 (34–32) (p.u.)	0.9	1.1	0.9464	0.9524	0.9592	0.9447	1.005	1.0316	0.9011	0.9092	0.9443	0.9049
T54 (11–41) (p.u.)	0.9	1.1	0.9276	0.9401	0.9196	0.9137	0.915	0.9504	0.9071	0.9054	0.9293	0.9163
T58 (15–45) (p.u.)	0.9	1.1	0.9504	1.003	0.9645	0.9417	0.93	1.0672	0.9016	0.9165	0.9012	0.9955
T59 (14–46) (p.u.)	0.9	1.1	0.9461	0.9966	0.98	0.9488	0.9151	1.0377	0.9022	0.9018	0.9016	0.9114
T65 (10–51) (p.u.)	0.9	1.1	0.9736	1.045	0.9772	1.0075	0.9595	1.0966	0.9019	0.9193	0.9501	0.927

Table 11 continued

Control parameters	Min.	Max.	CASE 1 [CODTBO]	CASE 1 [DTBO]	CASE 2 [CODTBO]	CASE 2 [DTBO]	CASE 3 [CODTBO]	CASE 3 [DTBO]	CASE 4 [CODTBO]	CASE 4 [DTBO]	CASE 5 [CODTBO]	CASE 5 [DTBO]
T66 (13–49) (p.u.)	0.9	1.1	0.9237	0.9791	0.9456	0.9132	0.9086	1.0444	0.902	0.9046	0.9173	0.904
T71 (11–43) (p.u.)	0.9	1.1	0.9351	0.9126	0.9597	0.9474	0.911	0.9264	0.9015	0.9087	0.9441	0.9275
T73 (40–56) (p.u.)	0.9	1.1	0.9595	0.9178	1.086	0.9485	1.0093	1.033	1.0614	1.0855	1.0697	1.0969
T76 (39–57) (p.u.)	0.9	1.1	0.9857	0.9016	0.9752	0.9357	0.9686	0.9547	1.0806	1.0931	1.0909	1.0844
T80 (9–55) (p.u.)	0.9	1.1	0.9041	1.0887	0.9408	0.9335	0.9468	1.0402	0.9012	0.904	0.9135	0.9363
QC18 (MVAr)	0	0.05	0.0491	0.0368	0.0313	0.0325	0.0159	0.0206	0.0498	0.0461	0.0053	0.0155
QC25 (MVAr)	0	0.05	0.0458	0.0397	0.04	0.041	0.0461	0.0289	0.044	0.0426	0.0467	0.0454
QC53 (MVAr)	0	0.05	0.0431	0.0469	0.035	0.0492	0.0466	0.0463	0.0376	0.0303	0.0431	0.0357
H9 (MWth)	10	35	34.4674	33.128	21.6296	17.7678	34.5337	27.7161	21.7295	23.1643	34.9734	29.518
H12 (MWth)	10	35	33.6865	33.7395	24.6519	19.7537	128.3428	33.9755	14.2055	12.6524	31.5354	32.3803
H58 (MWth)	0	2695.2	106.8461	108.1325	128.7184	137.4785	12.1235	113.3084	139.065	139.1833	108.4912	113.1016
Total cost ($/h)			30,863.9779	31,876.8012	42,685.9263	42,773.7183	31,161.2468	32,919.7796	42,752.5738	43,851.9257	32,347.5352	33,828.4241
Thermal cost ($/h)			14,591.8855	15,585.6035	16,630.079	16,690.7934	13,981.2973	14,065.1472	16,722.2246	18,418.1057	14,785.3148	13,074.3397
CHP cost ($/h)			14,673.4243	14,679.4336	24,217.407	24,138.2563	16,199.9852	17,188.9062	24,065.8191	23,467.8006	15,946.7827	19,090.5532
HOU cost ($/h)			1598.6681	1611.7642	1838.4403	1944.6685	979.9643	1665.7262	1964.5301	1966.0194	1615.4377	1663.5313
Emission ((t/h)			2.6326	2.7047	1.7585	1.7641	2.5114	2.5318	2.641	2.8638	2.7034	2.5919
Ploss (MW)			260.56	259.5	236.63	239.05	256.41	266.91	298.41	299.91	293.69	293.28
Voltageprofile (p.u)			4.1188	6.8725	5.0424	3.8374	3.6839	6.3445	4.467	4.0315	2.9781	2.614
L-index			0.3802	0.4655	0.4077	0.3748	0.3726	0.4652	0.2391	0.2443	0.2584	0.2605

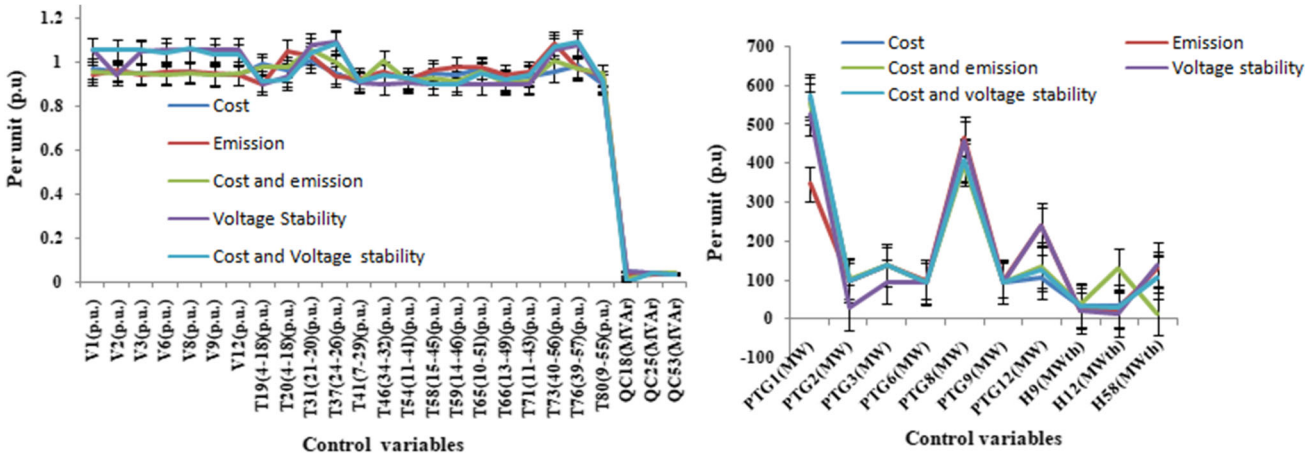

Fig. 6 Optimal value of control variables for case 1 to case 5 of test system-1 using CODTBO technique

Table 12 An overview of IEEE 57 bus system for wind–solar–EV based CHPED–OPF

Items	Quantity	Details
Buses	57	[ref]
Branches	80	[ref]
Thermal generators	5	5 power only units (buses 1,2, 3, 6 and 8), 2 CHP units (buses 9, and 12) and 1 heat only unit
Wind generators (WG1)	1	Buses:2
Solar unit (PV)	1	Buses:3
Electric vehicle (EV)	1	Buses:6
Tap changing transformer	15	Branches:19, 20, 31, 37, 41, 46, 54, 58, 59, 65, 66, 71, 73, 76 and 80
		Scheduled real power for 6 Nos. generators:
Control variables	34	Bus voltages of all generator buses (7 Nos.) transformer tap setting (15 nos), and compensation devices (3 nos), 3 heat units.
Load demand, Heat demand		1250.8 MW, 336.4 MVAr, 175 MWth
Range of load bus voltage	24	[0.94–1.06] p.u.
Compensation devices	3	Buses:18, 25 and 53

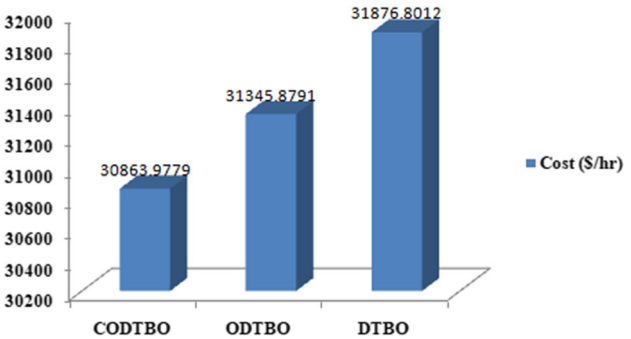

Fig. 7 Cost comparison study for test system-1 of CHPED-based OPF

5.3.2 Test system-3

Additionally EV also integrated with wind and solar, on CHPED-based OPF system to judge the performances of proposed CODTBO technique on more nonlinear-based system. Again use of more renewable sources, utility of thermal units get reduces which cause optimal solution over cost and emission during power generation. In this proposed wind–solar–EV-based IEEE-57 bus system wind unit is connected with on bus number 2, solar is connected with bus 3 and EV on bus 6. The total amount of load demand is 1250.8 MW MW, whereas reactive power and heat demand are 336.4 MVar and 175 MWth. An overview of IEEE 57 bus system for wind–solar–EV-based OPF-CHPED is depicted in Table 12. The simulation results of DTBO and CODTBO and optimal setting of control variables are illustrated in Table 14. The DTBO, ODTBO and CODTBO has been applied on the proposed renewable-based CHPED–OPF system and analogy study to judge the excellency of the proposed optimization method on single objective and multi-objective functions. The obtained optimal cost on wind–solar–EV-based system

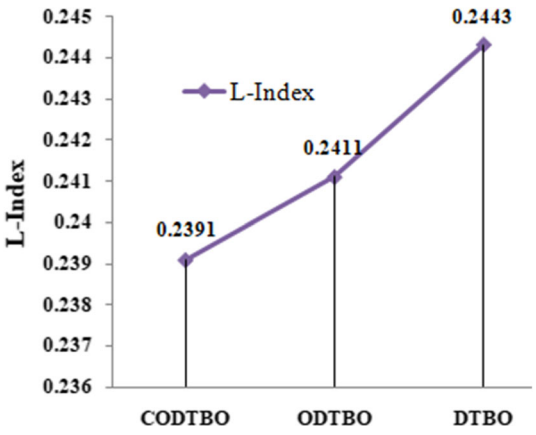

Fig. 8 Comparison study of stability index for test system-1 of CHPED-based OPF

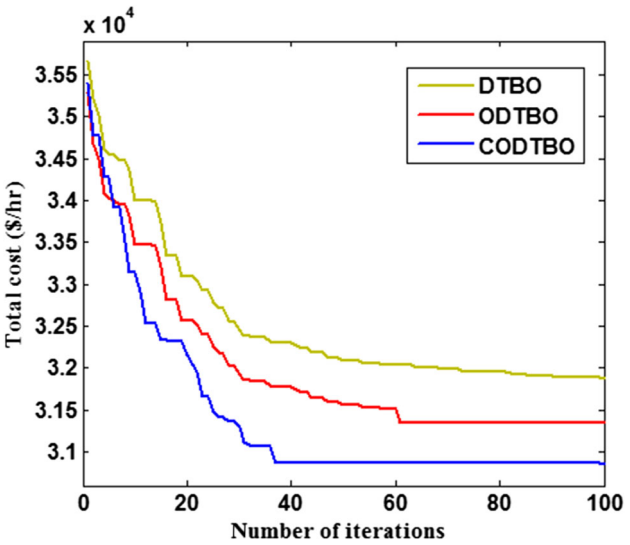

Fig. 9 Cost convergence graph for test system-1 of CHPED-based OPF

using CODTBO is 29,791.3288 $/h, emission 1.6053 (t/h), and reduced L-index is 0.235, whereas for multi-objective function simultaneously minimized cost and emission are 29,917.7694 $/h and 2.4244 (t/h). After that simultaneously minimized cost with stability index are 31,241.7366 $/h and 0.2545 . The obtained results using CODTBO technique are much better than other tested optimization techniques which is the evidence of superiority of CODTBO optimization technique. The statistical analysis has been done using DTBO, ODTBO and CODTBO on a renewable-based OPF-CHPED system and displayed in Table 13 which is the evidence of the robustness of the proposed CODTBO technique. The different comparison of CHPED-based OPF system on cost is displayed in Fig. 12. The convergence characteristics of different objective functions are shown in Fig. 13. When the CODTBO optimisation method, unlike the DTBO and ODTBO optimisation procedures, achieves results in all circumstances that smoothly converge to the optimal value in less than 30 iterations. From the above discussion it has been proved that the effectiveness of CODTBO technique is much better than other tested techniques.

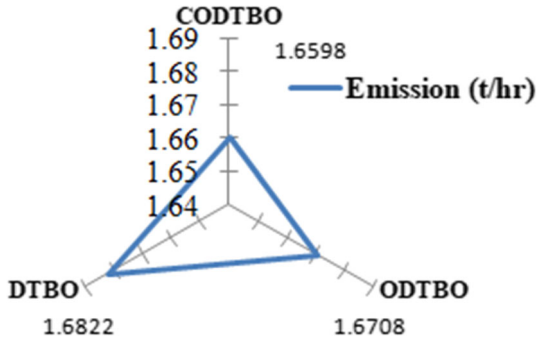

Fig. 10 Emission comparison study of wind–solar-based CHPED–OPF

The comparison of minimum cost using CODTBO for three different test systems is displayed in Fig. 14 where it has been observed the cost get reduces with incorporating more number of renewable sources (RESs). The voltage profile for without and with renewable-based CHPED–OPF has been displayed in Fig. 15 where it has been observed that voltage deviation is improved in wind–solar–EV-based CHPED–OPF system than other systems using CODTBO technique. From above discussion it has been proved that proposed CODTBO technique can deal with more nonlinear functions. It is the evidence of superiority of the proposed CODTBO technique (Table 15).

6 Conclusions and future scopes

In this paper, the main goal of this presentation is to illustrate how to schedule CHPED-based OPF using renewable energy sources and to show how effective the CODTBO optimisation technique is to fulfill the load demand for economic generation, less emission and less power losses with maintaining the load bus voltages within permissible limits. The main contributions of the proposed work are listed below:

- Integrating optimal power flow (OPF) in CHPED system
- Scheduling OPF-based CHPED with wind–solar–EVs.
- Solving both single- and multi-objective functions using newly developed CODTBO approach.
- Implementation of CODTBO in IEEE CEC benchmark functions

In the first part of the simulation study, it is found that use of CODTBO has significantly reduced the fuel cost with emission and fuel cost with L-index simultaneously for single- and multi-objective functions in comparison with

Table 13 Simulation results and control parameters of different cases for CHPED based OPF system of IEEE-57 bus with wind–solar

Control Parameters	Min.	Max.	CASE 6 [CODTBO]	CASE 6 [DTBO]	CASE 7 [CODTBO]	CASE 7 [DTBO]	CASE 8 [CODTBO]	CASE 8 [DTBO]	CASE 9 [CODTBO]	CASE 9 [DTBO]	CASE 10 [CODTBO]	CASE 10 [DTBO]
PTG1 (MW)	0	575.88	571.89	575.06	318.76	321.41	558.22	563.61	572	574.79	573.36	567.76
PW2 (MW)	30	100	96.84	98.46	96.96	99.99	99.93	96.9	43.21	31.39	96.96	98.82
PPV3 (MW)	40	140	138.27	138.04	139.34	137.66	138.74	138.95	73.26	44.99	137.6	135.28
PTG6 (MW)	30	100	99.32	97.59	98.62	96.89	98.46	96.38	94.11	94.04	96.34	99.12
PTG8 (MW)	100	550	396.84	357.72	493.55	496.43	406.36	410.1	444.84	473.94	423.15	431.27
PTG9 (MW)	30	100	96.47	94.67	99.58	99.87	95.58	96.91	98.67	99.55	96.37	94.16
PTG12 (MW)	100	410	116.09	151.12	239.5	241.22	114.57	114.25	225.53	244.19	121.87	121.59
V1 (p.u.)	0.94	1.06	0.9952	0.9657	0.9421	0.9476	0.9852	1.0373	1.0597	1.0473	1.0523	1.0555
V2 (p.u.)	0.94	1.06	1.0096	0.9705	0.9416	0.9446	0.9734	1.01	0.9582	0.9571	1.0393	1.0417
V3 (p.u.)	0.94	1.06	0.9696	0.9878	0.9446	0.9728	0.9476	0.9423	1.0584	1.0588	1.0468	1.0512
V6 (p.u.)	0.94	1.06	0.9779	0.9712	0.9608	0.9785	0.9421	0.9441	1.0575	1.06	1.0413	1.0449
V8 (p.u.)	0.94	1.06	0.9432	0.9539	0.9529	0.9787	0.9705	0.9432	1.0539	1.0543	1.0556	1.0432
V9 (p.u.)	0.94	1.06	0.9419	0.951	0.9476	0.9532	0.9554	0.9422	1.0549	1.0597	1.0394	1.0542
V12 (p.u.)	0.94	1.06	0.9414	0.9419	0.941	0.9548	0.9439	0.9451	1.0589	1.0599	1.0429	1.0493
T19 (4–18) (p.u.)	0.9	1.1	0.9731	1.0327	0.9566	1.0903	0.92	1.0298	0.9022	0.9155	0.9107	0.9072
T20 (4–18) (p.u.)	0.9	1.1	0.9211	0.9708	0.9451	1.0652	0.9241	1.0598	0.9048	0.9084	0.9023	0.9282
T31 (21–20) (p.u.)	0.9	1.1	0.9897	0.9378	0.956	0.9546	0.9453	0.947	1.1	7.4277	1.0832	1.0985
T37 (24–26) (p.u.)	0.9	1.1	0.9949	0.9245	0.9368	0.992	0.9659	0.9791	1.0942	1.0931	1.0827	1.0803
T41 (7–29) (p.u.)	0.9	1.1	1.0116	0.955	0.924	0.9919	0.9366	0.995	0.9004	0.9118	0.9068	0.9204
T46 (34–32) (p.u.)	0.9	1.1	1.0131	0.9075	0.9424	0.9502	1.0224	1.095	0.9003	0.9142	0.9023	0.9154
T54 (11–41) (p.u.)	0.9	1.1	0.9326	0.9019	0.9137	1.0616	0.9419	0.9306	0.9003	0.9093	0.9056	0.9014
T58 (15–45) (p.u.)	0.9	1.1	1.0259	1.0476	0.988	1.0439	0.9204	1.0192	0.9079	0.9012	0.9315	0.9026
T59 (14–46) (p.u.)	0.9	1.1	0.9985	1.048	0.9844	1.0561	0.9728	1.0774	0.9037	0.9017	0.9124	0.9407
T65 (10–51) (p.u.)	0.9	1.1	1.0236	1.062	1.0231	0.9978	0.9673	1.0527	0.9112	0.9027	0.9155	0.9458
T66 (13–49) (p.u.)	0.9	1.1	0.9622	0.9833	0.9569	0.996	0.929	0.991	0.9022	0.9008	0.9087	0.94

Table 13 continued

Control Parameters	Min.	Max.	CASE 6 [CODTBO]	CASE 6 [DTBO]	CASE 7 [CODTBO]	CASE 7 [DTBO]	CASE 8 [CODTBO]	CASE 8 [DTBO]	CASE 9 [CODTBO]	CASE 9 [DTBO]	CASE 10 [CODTBO]	CASE 10 [DTBO]
T71 (11–43) (p.u.)	0.9	1.1	0.9371	0.9358	0.9252	1.0355	1.0073	0.9582	0.9009	0.9034	0.9076	0.9093
T73 (40–56) (p.u.)	0.9	1.1	0.9994	0.9193	0.9607	0.9726	1.0319	1.0537	1.0991	1.0966	1.082	1.0916
T76 (39–57) (p.u.)	0.9	1.1	0.9069	0.9395	0.9168	1.0828	0.9588	0.9869	1.0907	1.098	1.0397	1.0903
T80 (9–55) (p.u.)	0.9	1.1	1.0473	0.9604	0.9453	0.9301	0.9472	1.0387	0.9023	0.9124	0.908	0.9538
QC18 (MVAr)	0	0.05	0.0107	0.0211	0.0261	0.0035	0.042	0.0379	0.0496	0.0492	0.0196	0.0454
QC25 (MVAr)	0	0.05	0.0186	0.0243	0.0474	0.0496	0.0278	0.0334	0.0489	0.05	0.0481	0.049
QC53 (MVAr)	0	0.05	0.0376	0.0022	0.0499	0.038	0.0467	0.0385	0.0495	0.0454	0.0498	0.05
H9 (MWth)	10	35	34.2646	32.6684	18.6575	27.4893	26.7069	32.6148	21.0364	13.6375	33.8873	32.3582
H12 (MWth)	10	35	28.3435	34.9795	32.0552	19.3714	33.8796	30.6808	12.2667	12.142	42.0547	34.1447
H58 (MWth)	0	2695.2	112.3919	107.3521	124.2872	128.1394	114.4134	111.7044	141.6969	149.2205	99.058	108.4971
Total cost ($/h)			30,057.0093	30,237.2572	43,235.6213	43,615.3749	30,337.5731	30,589.546	40,461.6974	43,789.0412	31,654.4568	32,018.1764
Thermal cost ($/h)			12,877.536	11,009.9126	16,993.2269	17,182.9381	13,277.4267	13,497.524	15,443.8958	17,156.3537	14,250.0622	14,668.9877
Wind cost ($/h)			65.443	66.9749	65.5521	68.4353	68.3818	65.498	26.5275	23.8636	65.5592	67.3171
Solar cost ($/h)			275.6738	275.2084	277.8098	274.4519	276.6134	277.0307	145.6654	89.1108	274.3355	269.6887
CHP cost ($/h)			15,182.334	17,281.357	24,112.1054	24,257.9259	15,037.6407	15,100.7072	22,847.706	24,423.5088	15,542.4298	15,396.6845
HOU cost ($/h)			1656.0225	1603.8043	1786.9271	1831.6239	1677.5104	1648.7861	1997.9027	2096.2043	1522.0702	1615.4983
Emission ((t/h)			2.5313	2.5551	1.6598	1.6822	2.4672	2.5145	2.7784	2.9289	2.6274	2.6176
Ploss (MW)			264.93	261.86	235.51	242.67	261.06	266.29	300.82	297.18	294.84	297.19
VD (p.u.)			6.3106	6.1651	5.1485	6.8219	4.397	7.6227	4.6587	4.5742	3.3023	2.9352
L-index			0.464	0.451	0.4159	0.4589	0.403	0.5233	0.2362	0.2379	0.2521	0.2571

Table 14 Simulation results and control parameters of different cases for CHPED based OPF system of IEEE-57 bus with wind–solar–EV

Control Parameters	Min.	Max.	CASE 11 [CODTBO]	CASE 11 [DTBO]	CASE 12 [CODTBO]	CASE 12 [DTBO]	CASE 13 [CODTBO]	CASE 13 [DTBO]	CASE 14 [CODTBO]	CASE 14 [DTBO]	CASE 15 [CODTBO]	CASE 15 [DTBO]
PTG1 (MW)	0	575.88	569.16	558.62	340.14	334.21	573.07	569.49	572.1	571.79	570.15	574.89
PW2 (MW)	30	100	98.61	99.74	99.93	99.4	94.57	96	42.46	37.64	92.93	98.97
PPV3 (MW)	40	140	138.93	138.74	139.64	136.96	139.53	134.98	41.07	52.79	137.63	139.71
PEV6 (MW)	30	100	98.75	98.45	98.05	99.19	99.7	99.46	98.03	91.68	99.72	99.35
PTG8 (MW)	100	550	406.1	373.6	469.5	483.57	368.57	352.74	467	464.04	443.61	430.09
PTG9 (MW)	30	100	95.11	97.05	98.86	99.69	99.28	94.26	98.78	97.85	76.75	98.52
PTG12 (MW)	100	410	106.86	140.23	240.15	238.84	135.69	158.77	234.38	237.53	104.67	105.73
V1 (p.u.)	0.94	1.06	0.9594	0.9417	0.9402	0.9561	0.9551	0.9472	1.0596	1.0561	1.044	1.0452
V2 (p.u.)	0.94	1.06	0.9529	0.9512	0.9481	0.9605	0.9661	0.9454	0.9502	0.9451	1.0523	1.0317
V3 (p.u.)	0.94	1.06	0.945	0.9416	0.944	0.953	0.9472	0.9527	1.0598	1.0593	1.0598	1.0383
V6 (p.u.)	0.94	1.06	0.9489	0.9435	0.9563	0.9725	0.9499	0.944	1.0569	1.0588	1.0505	1.0527
V8 (p.u.)	0.94	1.06	0.9503	0.9476	0.9567	0.9595	0.9497	0.951	1.0575	1.0599	1.0596	1.0524
V9 (p.u.)	0.94	1.06	0.9524	0.9437	0.9449	0.9645	0.9401	0.9425	1.053	1.0573	1.0426	1.0573
V12 (p.u.)	0.94	1.06	0.9555	0.9407	0.9449	0.9506	0.9584	0.9412	1.0587	1.0532	1.003	1.0324
T19 (4–18) (p.u.)	0.9	1.1	0.9142	0.9168	1.0896	1.0957	0.9891	0.9067	0.9006	0.9215	0.9259	0.9317
T20 (4–18) (p.u.)	0.9	1.1	0.9193	1.0696	0.9392	0.9157	0.9043	0.9152	0.9075	0.9148	0.9212	0.935
T31 (21–20) (p.u.)	0.9	1.1	0.9183	1.035	1.0722	0.9493	0.96	0.9544	1.0946	1.0971	1.0782	1.0788
T37 (24–26) (p.u.)	0.9	1.1	0.9467	0.9752	0.9174	1.0207	0.9451	0.9482	1.0997	1.0981	1.0872	1.0875
T41 (7–29) (p.u.)	0.9	1.1	0.995	0.9467	0.902	1.0336	0.911	0.9243	0.9053	0.9025	0.9159	0.9221
T46 (34–32) (p.u.)	0.9	1.1	0.9892	0.9831	0.9682	0.9375	0.9726	0.9711	0.903	0.9078	0.9011	0.911
T54 (11–41) (p.u.)	0.9	1.1	0.9201	0.925	0.9023	0.9538	1.0142	0.9315	0.9019	0.9027	0.9069	0.9008
T58 (15–45) (p.u.)	0.9	1.1	1.0129	0.9687	0.9527	1.0002	0.9559	0.9524	0.9001	0.9026	0.9006	0.905
T59 (14–46) (p.u.)	0.9	1.1	1.0448	0.9847	0.9596	1.0229	0.9996	0.9448	0.9005	0.901	0.9012	0.9309
T65 (10–51) (p.u.)	0.9	1.1	1.0917	1.0183	0.9852	1.0797	1.0206	0.9974	0.9	0.9015	0.9116	0.9072

Table 14 continued

Control Parameters	Min.	Max.	CASE 11 [CODTBO]	CASE 11 [DTBO]	CASE 12 [CODTBO]	CASE 12 [DTBO]	CASE 13 [CODTBO]	CASE 13 [DTBO]	CASE 14 [CODTBO]	CASE 14 [DTBO]	CASE 15 [CODTBO]	CASE 15 [DTBO]
T66 (13–49) (p.u.)	0.9	1.1	0.9819	0.95	0.932	0.9948	0.9344	0.931	0.9029	0.9022	0.9026	0.9133
T71 (11–43) (p.u.)	0.9	1.1	0.9092	0.9565	0.9055	0.9535	0.9338	0.9249	0.9015	0.9019	0.9214	0.9066
T73 (40–56) (p.u.)	0.9	1.1	0.9079	0.9714	0.9061	0.939	1.0169	0.9929	1.0999	1.0992	1.0497	1.0934
T76 (39–57) (p.u.)	0.9	1.1	0.9009	0.9096	0.9403	0.9104	0.9628	0.9429	1.099	1.0924	1.0725	1.0931
T80 (9–55) (p.u.)	0.9	1.1	1.0369	1.0224	0.9215	1.0897	0.9302	0.9531	0.9006	0.9117	0.9082	0.9097
QC18 (MVAr)	0	0.05	0.0003	0.0491	0.0072	0.001	0.0438	0.0048	0.0487	0.0485	0.0369	0.0418
QC25 (MVAr)	0	0.05	0.0482	0.0405	0.0473	0.0475	0.0479	0.0479	0.0488	0.0488	0.0462	0.0456
QC53 (MVAr)	0	0.05	0.0256	0.0469	0.05	0.0446	0.0391	0.0253	0.0497	0.0426	0.0169	0.0456
H9 (MWth)	10	35	32.7246	34.8329	30.9436	27.1971	32.3622	34.9162	29.9319	30.1865	34.587	31.3983
H12 (MWth)	10	35	34.35	34.5319	24.8766	25.2582	34.1299	34.3284	18.0602	28.5369	34.5489	34.1007
H58 (MWth)	0	2695.2	107.9254	105.6352	119.1798	122.5447	108.5079	105.7553	127.0078	116.2766	105.8641	109.501
Total cost ($/h)			29,791.3288	30,218.7013	41,748.9181	42,528.1486	29,917.7694	30,363.6654	42,206.2259	42,168.3104	30,732.5607	31,241.7366
Thermal cost ($/h)			13,085.5324	11,415.8115	15,371.8708	16,194.542	11,262.7111	10,507.4317	16,494.129	16,318.2738	15,129.4053	14,400.4428
Wind cost ($/h)			67.1214	68.2012	68.3818	67.8733	63.3038	64.6472	26.2717	24.8925	61.7789	67.4587
Solar cost ($/h)			277.0015	276.6134	278.4229	273.0489	278.1884	269.1002	81.27	104.7131	274.3944	278.551
EV cost ($/h)			158.4103	157.8139	157.019	159.2956	160.3269	159.8317	156.9811	144.2753	160.3689	159.6197
CHP cost ($/h)			14,593.6163	16,713.8053	24,143.8199	24,066.3099	16,537.6298	17,774.992	23,629.1965	23,878.5661	13,517.8574	14,709.8309
HOU cost ($/h)			1609.6467	1586.456	1729.4037	1767.0788	1615.6096	1587.6627	1818.3777	1697.5895	1588.7557	1625.8335
Emission ((t/h)			2.4965	2.3424	1.6053	1.6356	2.4244	2.3682	2.8335	2.8237	2.6236	2.6167
Ploss (MW)			262.79	255.63	235.47	241.05	259.61	254.93	303.01	302.51	295.36	296.46
VD (p.u.)			6.8141	6.0532	4.4906	6.7106	4.9685	4.5125	4.769	4.6393	3.2145	3.1612
L-index			0.4855	0.4364	0.3957	0.4553	0.4096	0.3987	0.235	0.2363	0.2519	0.2545

Table 15 Statistical analysis of three test systems

Case		CODTBO	ODTBO	DTBO			CODTBO	ODTBO	DTBO
Case 1	Best (min)	30,863.9779	31,345.8791	31,876.8012	Case 9	Best (min)	0.2362	0.2369	0.2379
	Mean (average)	30,865.7865	31,350.4321	31,895.0916		Mean (average)	0.2411	0.2766	0.2887
	Median	30,864.2391	31,351.0021	31,896.0129		Median	0.2498	0.2897	0.3211
	Worst (max)	30,869.5649	31,357.9001	31,917.9801		Worst (max)	0.2919	0.3465	0.3997
	Standard deviation	1.6109	2.8901	10.0231		Standard deviation	0.0019	0.0198	0.0254
Case 2	Best (min)	1.7585	1.7613	1.7641	Case 10	Best (min)	34,175.4568	34,334.8872	34,589.1764
	Mean (average)	1.7605	1.7987	1.8321		Mean (average)	34,179.5593	34,342.6721	34647.1 432
	Median	1.7598	1.8096	1.8432		Median	34,179.8921	34,343.0023	34,649.6655
	Worst (max)	1.7635	1.8156	1.9543		Worst (max)	34,184.0176	34,351.4539	34,704.9845
	Standard deviation	0.0017	0.0211	0.0432		Standard deviation	2.0012	3.8791	28.9823
Case 3	Best (min)	33,672.6468	33,785.0273	33,922.3114	Case 11	Best (min)	29,791.3288	29,901.8921	30,218.7013
	Mean (average)	33,676.0065	33,794.9871	33,944.0045		Mean (average)	29,792.2239	29,904.3329	30,228.8751
	Median	33,675.7012	33,793.0034	33,945.3041		Median	29,793.0001	29,905.3211	30,229.4501
	Worst (max)	33,681.1341	33,804.7871	33,976.8761		Worst (max)	29,793.9851	29,907.9983	30,240.0021
	Standard deviation	2.3404	4.4302	11.1207		Standard deviation	0.4577	1.5011	5.1943
Case 4	Best (min)	0.2391	0.2411	0.2443	Case 12	Best (min)	1.6053	1.6211	1.6356
	Mean (average)	0.2437	0.2664	0.3211		Mean (average)	1.6077	1.6409	1.6778
	Median	0.2438	0.2666	0.3098		Median	1.6101	1.6501	1.7002
	Worst (max)	0.2483	0.3128	0.4215		Worst (max)	1.6856	1.7643	1.8123
	Standard deviation	0.0023	0.0227	0.0384		Standard deviation	0.0011	0.0098	0.0211

Table 15 continued

Case		CODTBO	ODTBO	DTBO			CODTBO	ODTBO	DTBO
Case 5	Best (min)	34,931.5352	35,591.7721	36,433.4241	Case 13	Best (min)	32,342.1711	32,566.5007	32,731.8654
	Mean (average)	34,936.5643	35,604.6704	36,502.835		Mean (average)	32,344.8902	32,570.8922	32,742.7383
	Median	34,938.8766	35,606.8028	36,503.8711		Median	32,345.0819	32,471.6272	32,741.9831
	Worst (max)	34,976.0801	35,634.8764	36,576.9005		Worst (max)	32,348.8702	3278.0065	32,755.0092
	Standard deviation	2.6751	6.4492	34.871		Standard deviation	1.0972	2.0987	5.0056
Case 6	Best (min)	30057.0093	30131.7001	30,237.2572	Case 14	Best (min)	0.235	0.2358	0.2363
	Mean (average)	30,059.5632	30,135.3012	30,254.8711		Mean (average)	0.2382	0.2585	0.2695
	Median	30,060.2137	30,134.0098	30,256.0281		Median	0.2391	0.2592	0.2721
	Worst (max)	30,062.0056	30,138.5401	30,271.5412		Worst (max)	0.2401	0.3104	0.3298
	Standard deviation	1.0032	2.0921	8.4532		Standard deviation	0.0012	0.0113	0.0165
Case 7	Best (min)	1.6598	1.6708	1.6822	Case 15	Best (min)	33,251.5607	33,407.2011	33,786.7366
	Mean (average)	1.6627	1.7152	1.7466		Mean (average)	33,253.6784	33,412.0655	33,828.6991
	Median	1.6701	1.7164	1.7501		Median	33,254.0231	33,413.1199	33,829.2011
	Worst (max)	1.7145	1.8308	1.8645		Worst (max)	33,258.9856	33,418.0554	33,862.9845
	Standard deviation	0.0013	0.0156	0.03219		Standard deviation	0.9871	2.4321	20.9812
Case 8	Best (min)	32,804.7731	32,915.7811	33,104.046					
	Mean (average)	32,808.0904	32,921.9813	33,123.9871					
	Median	32,809.0102	32,922.7482	33,124.5437					
	Worst (max)	32,812.9832	32,930.8301	33,145.9283					
	Standard deviation	1.9754	3.0706	8.9831					

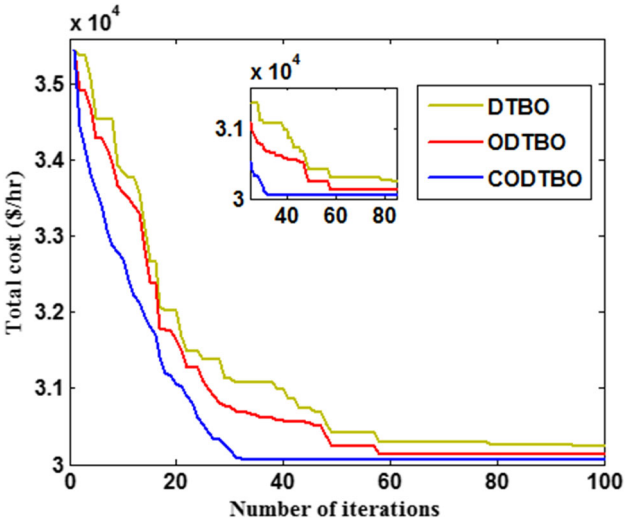

Fig. 11 Cost convergence graph for test system-2 of CHPED-based OPF with wind and solar

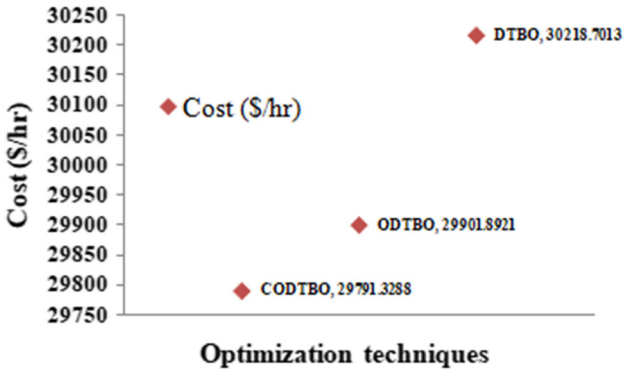

Fig. 12 Cost comparison study for test system-3 of CHPED based OPF with wind–solar–EV)

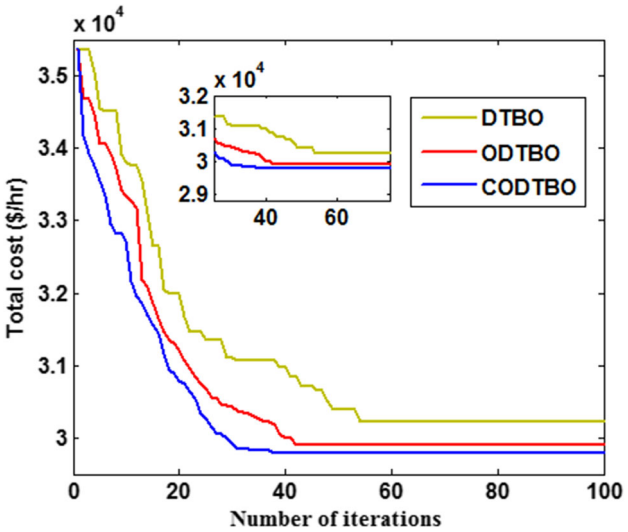

Fig. 13 Cost convergence graph for test system-3 of CHPED based OPF with wind, solar and EV

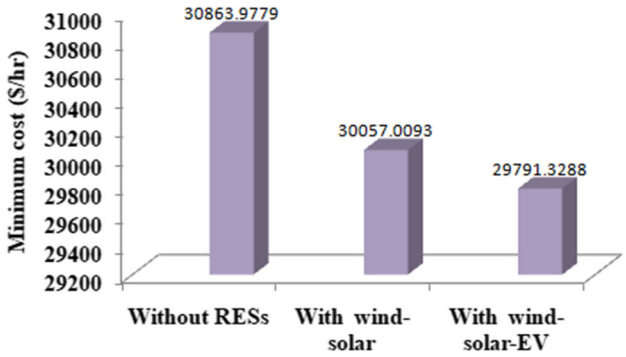

Fig. 14 Different test systems result using CODTBO technique)

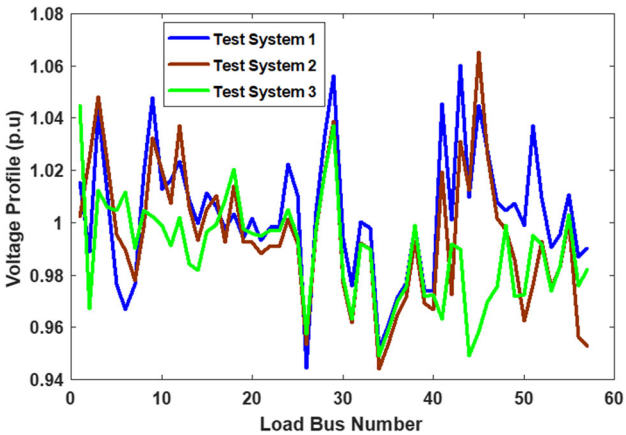

Fig. 15 Voltage profile for three different test systems using CODTBO technique

other optimization techniques and all the system constrains are also been satisfied. The overall fuel cost and emission are lowered by 3.48% and 5.1%, respectively, and the L-index is enhanced by 21.6% in the second phase when wind–solar–EVs are integrated with CHPED–OPF. It has been established that the suggested CODTBO can effectively handle nonlinear functions as a result. The fuel cost is further decreased by 1.65% and computational speed is increased by 45% when chaotic-oppositional-based learning (CO) is combined with DTBO (CODTBO). Henceforth, CODTBO has the better exploration capability and better searching ability due to improved version of DTBO. The proposed wind–solar–EV with CHPED-based OPF brings both environmental benefits and economic operation to the power grid. By doing statistical analysis on three systems with obtaining least variation of mean and optimal values of cost, emission and voltage deviation with the tolerance of less than 0.025%, the robustness of the suggested CODTBO has been judged. Thus, it may be concluded that the CODTBO is much superior to the other tested optimization techniques in all respect. In future it may be extended to more nonlinear-based system and may be applied on real-time-based problems for optimal solution.

Author Contributions "Literature review is done by Chandan Paul and Tushnik sarkar; Algorithm is performed by Provas Kumar Roy and Susanta Dutta; Data collection is done by Chandan Paul; Simulation results with analysis are executed by Chandan Paul; Editing of the manuscript is done by Provas Kumar Roy and finally, all authors read and approved the final manuscript."

Funding Not applicable.

Data Availability Statement The data that support the findings of this study are available on request from the corresponding author.

Declarations

Conflict of interest The authors confirm that they have no noted competing economic concerns or particular communications which can be presented to determine the achievement recorded in the research paper.

Ethical approval The research paper does not incorporate several works with mortal fields or animals realized through either of the authors.

References

1. Sashirekha A, Pasupuleti J, Moin NH, Tan CS (2013) Combined heat and power (CHP) economic dispatch solved using Lagrangian relaxation with surrogate subgradient multiplier updates. Int J Electr Power Energy Syst 44(1):421–430
2. Thomson M, Twigg PM, Majeed BA, Ruck N (2000) Statistical process control based fault detection of CHP units. Control Eng Pract 8(1):13–20
3. Fortenbacher P, Demiray T (2019) Linear/quadratic programming-based optimal power flow using linear power flow and absolute loss approximations. Int J Electr Power Energy Syst 107:680–689
4. Pourakbari-Kasmaei M, Mantovani JRS (2018) Logically constrained optimal power flow: solver-based mixed-integer nonlinear programming model. Int J Electr Power Energy Syst 97:240–249
5. Leveringhaus T, Kluß L, Bekker I, Hofmann L (2022) Solving combined optimal transmission switching and optimal power flow sequentially as convexificated quadratically constrained quadratic program. Electr Power Syst Res 212:108534
6. Paul C, Roy PK, Mukherjee V (2022) Optimal solution of combined heat and power dispatch problem using whale optimization algorithm. Int J Appl Metaheuristic Comput (IJAMC) 13(1):1–26
7. Al-Betar MA, Awadallah MA, Makhadmeh SN, Doush IA, Zitar RA, Alshathri S, Elaziz MA (2023) A hybrid Harris Hawks optimizer for economic load dispatch problems. Alex Eng J 64:365–389
8. Dutta S, Roy PK, Nandi D (2015) Optimal location of UPFC controller in transmission network using hybrid chemical reaction optimization algorithm. Int J Electr Power Energy Syst 64:194–211
9. Kumar Roy P, Paul C (2015) Optimal power flow using Krill Herd algorithm. Int Trans Electr Energy Syst 25(8):1397–1419
10. Shaheen AM, Elsayed AM, Ginidi AR, El-Sehiemy RA, Elattar E (2022) A heap-based algorithm with deeper exploitative feature for optimal allocations of distributed generations with feeder reconfiguration in power distribution networks. Knowl Based Syst 241:108269
11. El-Fergany AA, Hasanien HM (2018) Tree-seed algorithm for solving optimal power flow problem in large-scale power systems incorporating validations and comparisons. Appl Soft Comput 64:307–316
12. Xiao H, Dong Z, Kong L, Pei W, Zhao Z (2018) Optimal power flow using a novel metamodel based global optimization method. Energy Procedia 145:301–306
13. Mukherjee A, Roy PK, Mukherjee V (2016) Transient stability constrained optimal power flow using oppositional Krill Herd algorithm. Int J Electr Power Energy Syst 83:283–297
14. Mandal B, Roy PK, and (2014) Multi-objective optimal power flow using quasi-oppositional teaching learning based optimization. Appl Soft Comput 21:590–606
15. Sunanda H, Kumar RP (2021) Solar–wind–hydro–thermal scheduling using moth flame optimization. Optimal Control Appl Methods 44(2):391–425
16. Paul C, Roy PK, Mukherjee V (2020) Chaotic whale optimization algorithm for optimal solution of combined heat and power economic dispatch problem incorporating wind. Renew Energy Focus 35:56–71
17. Chandan P, Provas KR, Vivekananda M (2021) Study of wind–solar based combined heat and power economic dispatch problem using quasi-oppositional-based whale optimization technique. Optimal Control Appl Methods 44:480–507
18. Paul C, Roy PK, Mukherjee V (2021) Application of chaotic quasi-oppositional whale optimization algorithm on CHPED problem integrated with wind–solar–EVs. Int Trans Electr Energy Syst 31(11):e13124
19. Zhang Z, Shang L, Liu C, Lai Q, Jiang Y (2023) Consensus-based distributed optimal power flow using gradient tracking technique for short-term power fluctuations. Energy 264:125635
20. Ida Evangeline S, Rathika P (2022) Wind farm incorporated optimal power flow solutions through multi-objective horse herd optimization with a novel constraint handling technique. Expert Syst Appl 194:116544
21. Li S, Gong W, Wang L, Qiong G (2022) Multi-objective optimal power flow with stochastic wind and solar power. Appl Soft Comput 114:108045
22. Chen T, Lam AYS, Song Y, Hill DJ (2022) Fast tuning of transmission power flow routers for transient stability constrained optimal power flow under renewable uncertainties. Electr Power Syst Res 213:108735
23. Sulaiman MH, Mustaffa Z, Rashid MIM (2023) An application of teaching–learning-based optimization for solving the optimal power flow problem with stochastic wind and solar power generators. Res Control Optim 10:100187
24. Basu M (2023) Dynamic optimal power flow for isolated microgrid incorporating renewable energy sources. Energy 264:126065
25. Naderi E, Mirzaei L, Trimble JP, Cantrell DA (2023) Multi-objective optimal power flow incorporating flexible alternating current transmission systems: application of a wavelet-oriented evolutionary algorithm. Electr Power Compon Syst 52:1–30
26. Naderi E, Mirzaei L, Pourakbari-Kasmaei M, Cerna FV, Lehtonen M (2023) Optimization of active power dispatch considering unified power flow controller: application of evolutionary algorithms in a fuzzy framework. Evol Intell 17:1–31
27. Naderi E, Pourakbari-Kasmaei M, Cerna FV, Lehtonen M (2021) A novel hybrid self-adaptive heuristic algorithm to handle single-and multi-objective optimal power flow problems. Int J Electr Power Energy Syst 125:106492
28. Alizadeh A, Kamwa I, Moeini A, Mohseni-Bonab SM (2023) Energy management in microgrids using transactive energy control concept under high penetration of renewables; a survey and case study. Renew Sustain Energy Rev 176:113161
29. He P, Pan Z, Fan J, Tao Y, Wang M (2023) Coordinated design of PSS and multiple FACTS devices based on the PSO-GA algorithm to improve the stability of wind–PV–thermal-bundled power system. Electr Eng 106

30. Kumar R, Sharma VK (2023) Interconnected power control on unequal, deregulated multi-area power system using three-degree-of-freedom-based FOPID-PR controller. Electr Eng 106
31. Biswas PP, Suganthan PN, Amaratunga GAJ (2017) Optimal power flow solutions incorporating stochastic wind and solar power. Energy Convers Manag 148:1194–1207
32. Dehghani M, Trojovská E, Trojovskỳ P (2022) A new human-based metaheuristic algorithm for solving optimization problems on the base of simulation of driving training process. Sci Rep 12(1):9924
33. Anantha P (1989) Energy function analysis for power system stability. Springer, New York
34. Awad NH, Ali MZ, Suganthan PN (2017) Problem definitions and evaluation criteria for the CEC 2017 special session and competition on single objective real-parameter numerical optimization. National University of Defense Technology, Changsha, Hunan, PR China and Kyungpook National University, Daegu, South Korea and Nanyang Technological University, Singapore, Technical Report
35. Derrac J, García S, Molina D, Herrera F (2011) A practical tutorial on the use of nonparametric statistical tests as a methodology for comparing evolutionary and swarm intelligence algorithms. Swarm Evol Comput 1(1):3–18